Check for updates

JIPB Journal of Integrative Plant Biology

Research Article
https://doi.org/10.1111/jipb.13193

Arabidopsis F-BOX STRESS INDUCED 4 is required to repress excessive divisions in stomatal development

Yi Li[1,2], Shan Xue[1,3], Qixiumei He[1,2], Junxue Wang[1,4], Lingling Zhu[1,2], Junjie Zou[1,5], Jie Zhang[1,2], Chaoran Zuo[1,2], Zhibin Fan[1,2], Junling Yue[1,2], Chunxia Zhang[1], Kezhen Yang[1]* and Jie Le[1,2]*

1. Key Laboratory of Plant Molecular Physiology, CAS Center for Excellence in Molecular Plant Sciences, Institute of Botany, The Chinese Academy of Sciences, Beijing 100093, China
2. University of Chinese Academy of Sciences, Beijing 100049, China
3. The Institute of Scientific and Technical Information of China, Beijing 100038, China
4. Wenbo School, Jinan 250100, China
5. Biotechnology Research Institute, Chinese Academy of Agricultural Sciences, Beijing 100081, China

*Correspondences: Kezhen Yang (ykzdsp@163.com); Jie Le (lejie@ibcas.ac.cn, Dr. Le is fully responsible for the distributions of the materials associated with this article)

Yi Li

Jie Le

ABSTRACT

During the terminal stage of stomatal development, the R2R3-MYB transcription factors FOUR LIPS (FLP/MYB124) and MYB88 limit guard mother cell division by repressing the transcript levels of multiple cell-cycle genes. In *Arabidopsis thaliana* possessing the weak allele *flp-1*, an extra guard mother cell division results in two stomata having direct contact. Here, we identified an ethylmethane sulfonate-mutagenized mutant, *flp-1 xs01c*, which exhibited more severe defects than *flp-1* alone, producing giant tumor-like cell clusters. *XS01C*, encoding F-BOX STRESS-INDUCED 4 (FBS4), is preferentially expressed in epidermal stomatal precursor cells. Overexpressing *FBS4* rescued the defective stomatal phenotypes of *flp-1 xs01c* and *flp-1* mutants. The deletion or substitution of a conserved residue (Proline166) within the F-box domain of FBS4 abolished or reduced, respectively, its interaction with Arabidopsis Skp1-Like1 (ASK1), the core subunit of the Skp1/Cullin/F-box E3 ubiquitin ligase complex. Furthermore, the FBS4 protein physically interacted with CYCA2;3 and induced its degradation through the ubiquitin-26S proteasome pathway. Thus, in addition to the known transcriptional pathway, the terminal symmetric division in stomatal development is ensured at the post-translational level, such as through the ubiquitination of target proteins recognized by the stomatal lineage F-box protein FBS4.

Keywords: cell division, cell cycle, F-BOX, stomatal development, ubiquitination

Li, Y., Xue, S., He, Q., Wang, J., Zhu, L., Zou, J., Zhang, J., Zuo, C., Fan, Z., Yue, J., Zhang, C., Yang, K., and Le, J. (2022). *Arabidopsis F-BOX STRESS INDUCED 4* is required to repress excessive divisions in stomatal development. J. Integr. Plant Biol. **64:** 56–72.

INTRODUCTION

Stomata are plant epidermal micro-valves which regulate gas exchange and water transpiration between plants and the environment (Casson and Hetherington, 2010). A stoma consists of a pair of mirror-symmetric guard cells (2-GCs) surrounding a pore, and the cell structure is important for stomatal movement in response to environmental changes. Stomata are derived from protodermal cells through a series of cell divisions and cell differentiation. The precursor meristemoid (M) mother cell (MMC) undergoes asymmetric division to produce the triangular M. The M differentiates into a guard mother cell (GMC), which generates a pair of GCs through a symmetric division. In past decades, major breakthroughs in our understanding of stomatal development have included the identification of multiple

© 2021 Institute of Botany, Chinese Academy of Sciences

transcription factors and their roles in cell fate decision, cell division, and cell differentiation. The basic Helix–Loop–Helix transcription factors play pivotal roles in regulating stomatal development. SPEECHLESS (SPCH) is critical for the asymmetric divisions (MacAlister et al., 2007; Pillitteri and Torii, 2012), MUTE controls the transition from M to GMC (Pillitteri et al., 2007), and FAMA is required for the terminal GMC division and GC differentiation that form a functional stomatal complex (Ohashi-Ito and Bergmann, 2006).

The R2R3-MYB transcription factor FOUR LIPS (FLP/MYB124) has a function similar to that of FAMA in regulating the terminal GMC division. In plants containing the weak allele *flp-1*, approximately 25% of stomata exist in pairs having direct contact, which leads to the formation of the four GC (4-GC) stomatal clustering phenotype (Lai et al., 2005). *MYB88* is a close paralog of *FLP*, but its mutation does not produce a stomatal phenotype. However, the *flp myb88* double mutant displays a more severe phenotype than the *flp* single mutant. In addition, *FLP* is a pleiotropic gene that participates in many other aspects of plant development and responses to abiotic stresses (Xie et al., 2010b; Makkena et al., 2012; Chen et al., 2015; Wang et al., 2015).

Both FLP and MYB88 control the stomatal terminal division through the transcriptional repression of cell-cycle genes, including *CYCLIN-DEPENDENT KINASE B1*s (*CDKB1*s), *CDKA;1*, and *CYCLIN A2*s (*CYCA2*s) (Xie et al., 2010a; Vanneste et al., 2011; Yang et al., 2014). Reducing the activities of CDKB1s or CDKA;1 leads to defective GMC division, resulting in the formation of single guard cells (SGCs) (Xie et al., 2010a; Yang et al., 2014). CDKB1s and CYCA2s form a functional CDK–CYCLIN complex to synergistically promote GMC division (Boudolf et al., 2009; Vanneste et al., 2011). Specifically elevating the transcriptional levels of *CDK*s and *CYCLIN*s at the late stage of stomatal development induces extra GC divisions. The CYCA2 expression levels are the rate limiting factors in the terminal division of stomatal development (Yang et al., 2014). The CDKB1-mediated phosphorylation of DNA replication protein A2 precisely controls the terminal division and DNA repair in plants, indicating that post-translational modifications are also important in GMC division (Yang et al., 2019).

The degradation of cyclins by E3 ubiquitin ligases is an important regulatory mechanism for cell-cycle transition from one stage to the next (Nakayama and Nakayama, 2005). In yeast, the C-type cyclin Ctk2p of the CTDK-I complex, which has been implicated in the phosphorylation of RNA polymerase II and in transcriptional control, can be rapidly degraded through the ubiquitin-proteasome pathway (Hautbergue and Goguel, 1999). In animals, cyclin A and cyclin B are ubiquitinated and degraded by Anaphase-Promoting Complex/Cyclosome $(APC/C)^{CDC20}$ in prometaphase and metaphase, respectively (den Elzen and Pines, 2001; Geley et al., 2001). In humans, cyclin D3 is polyubiquitinated via Skp1/Cullin/F-box $(SCF)^{Fbxl8}$ for degradation at the G1-to-S phase transition (Yoshida et al., 2021). Additionally, the APC^{Cdh1} and SCF^{Cdc4} complexes work together to ubiquitinate and degrade cyclin Clb6 during the G1-to-S phase transition in yeast, which suggests that multiple E3 ubiquitin ligases are coordinately involved in cyclin proteolysis during cell-cycle progression (Jackson et al., 2006; Wu et al., 2016).

In plants, the E3 ligases are classified into four types, Homologous to the E6-AP Carboxyl Terminus, Really Interesting New Gene, U-box, and Cullin-RING Ligase (CRL). However, the best-characterized plant E3s are the APC/C and SCF complexes of the CRLs, which are involved in almost all aspects of plant development (Ban and Estelle, 2021). In the model plant *Arabidopsis thaliana*, APC/C subunit 11 (APC11) ubiquitinates and promotes CYCB1;1 degradation, which is required for the initiation of the first zygotic division (Guo et al., 2016). CELL CYCLE SWITCH 52 (CCS52) proteins are activators of APC/C, and a mutation in *CCS52A1* enhances the stabilization of CYCA2;3-GFP (green fluorescent protein), leading to decreased endoreduplication and excessive cell divisions (Boudolf et al., 2009). ULTRAVIOLET-B-INSENSITIVE 4 (UVI4) is a specific inhibitor of $APC/C^{CCS52A1}$, and a mutation in *UVI4* results in the premature exit from the cell cycle and decreased numbers of meristematic cortex cells in roots (Heyman et al., 2011, 2017; Xu et al., 2016). CYCA3;4 is a target of $APC/C^{CCS52A2}$, and the lack of stomatal phenotypes in *CYCA3;4*-overexpression lines is partially counteracted by the co-overexpression of *CCS52A2*, indicating a role for $APC/C^{CCS52A2}$-mediated CYCA3;4 regulation in stomatal development (Willems et al., 2020).

Plant F-box proteins act as important components of the SCF complex (Fang and Weissman, 2004). F-box proteins interact with Skp1/ASK proteins through F-box domains and with their substrates through C-terminal protein–protein interaction domains (Hua and Vierstra, 2011). F-box proteins having F-box domain deletions are able to interact with their substrates, but are unable to mediate substrate degradation (Yaron et al., 1998). In addition, untethering F-box proteins from SCF complexes changes their stability (Yu et al., 2015). In *Arabidopsis*, there are nearly 700 F-box proteins, but only a small subset has been characterized in detail (Abd-Hamid et al., 2020). The E3 ubiquitin ligase CONSTITUTIVE PHOTOMORPHOGENIC1 degrades the SCREAM/ICE1 transcription factor in darkness, demonstrating the involvement of ubiquitination pathways in the modulation of stomatal development (Lee et al., 2017).

To further reveal the regulatory mechanisms involved in the FLP-mediated terminal division of stomatal development, an ethylmethane sulfonate-mutagenized *flp-1* population was used to discover novel components. In this study, we identified the mutant *flp-1 xs01c*, which had a severe defective stomatal phenotype compared with that of *flp-1*. *XS01C* encodes F-BOX STRESS-INDUCED 4 (FBS4), which is preferentially expressed in epidermal stomatal precursor cells. FBS4 interacted with Arabidopsis Skp1-Like1 (ASK1), the core subunit of the SCF E3 ubiquitin ligase complex, via its F-box domain. Furthermore, we demonstrated that FBS4 physically interacted with CYCA2;3 and induced its degradation via the ubiquitin-26S proteasome pathway. Thus, in addition to the known FLP-mediated transcriptional regulatory pathway, the terminal symmetric division of stomatal development is

verified at the post-translational level through the FBS4-mediated ubiquitination pathway.

RESULTS

A *XS01C* mutation aggravates the stomatal defects of *flp-1*

In contrast to the normal 2-GC stomata found in wild-type plants, approximately 30% of stomata in plants harboring the weak allele *flp-1* consist of four GCs in direct contact, forming a 4-GC stomatal cluster (Figure 1A, B). To identify novel components that influence *FLP*-dependent stomatal terminal divisions, we screened mutants from the ethylmethane sulfonate-mutagenized M_2 populations of *flp-1* by observing stomatal phenotypes. *flp-1 xs01c* was isolated because of its significantly enhanced *flp-1* stomatal phenotype. Unlike the formation of 4-GC stomatal clusters in *flp-1*, *flp-1 xs01c* produces giant tumor-like cell clusters having over-proliferative small and narrow epidermal cells, and 73.9% of the clusters consist of more than eight cells (Figure 1C, O).

To identify the fates of the over-proliferating cells in the *flp-1 xs01c* epidermis, stomatal lineage- and stage-specific reporters were introduced into the *flp-1 xs01c* double mutant by crossing. *TOO MANY MOUTHS* (*TMM*) is expressed throughout stomatal lineages, but not in pavement cells and mature GCs (Nadeau and Sack, 2002). Most of the dividing cells within *flp-1 xs01c* tumors exhibited TMM-GFP signals, confirming that the tumor cells had stomatal lineage cell fates but most of them failed to reach the mature GC stage (Figure 1D, E). *FAMA:GFP* was strongly expressed in late GMCs and young GCs (YGCs), but the level gradually decreased in mature GCs. Within the *flp-1 xs01c* tumors, most cells expressed FAMA:GFP, indicating their GMC/YGC identity (Figure 1F, G). In the older cotyledons of *flp-1 xs01c*, continuous cell overproliferation resulted in the enlargement of tumors (Figure 1G inset).

Similar to *FAMA*, *FLP* is specifically expressed in late GMCs that are about to divide and in newly formed YGCs. In the *flp-1 xs01c* mutant, *FLP:GUS* was highly expressed in tumor cells. The expression of *FLP:GUS* in the *flp-1 xs01c* tumors indicates that *FLP* and *XS01C* are not absolutely required for *FLP* expression (Figure 1H, I).

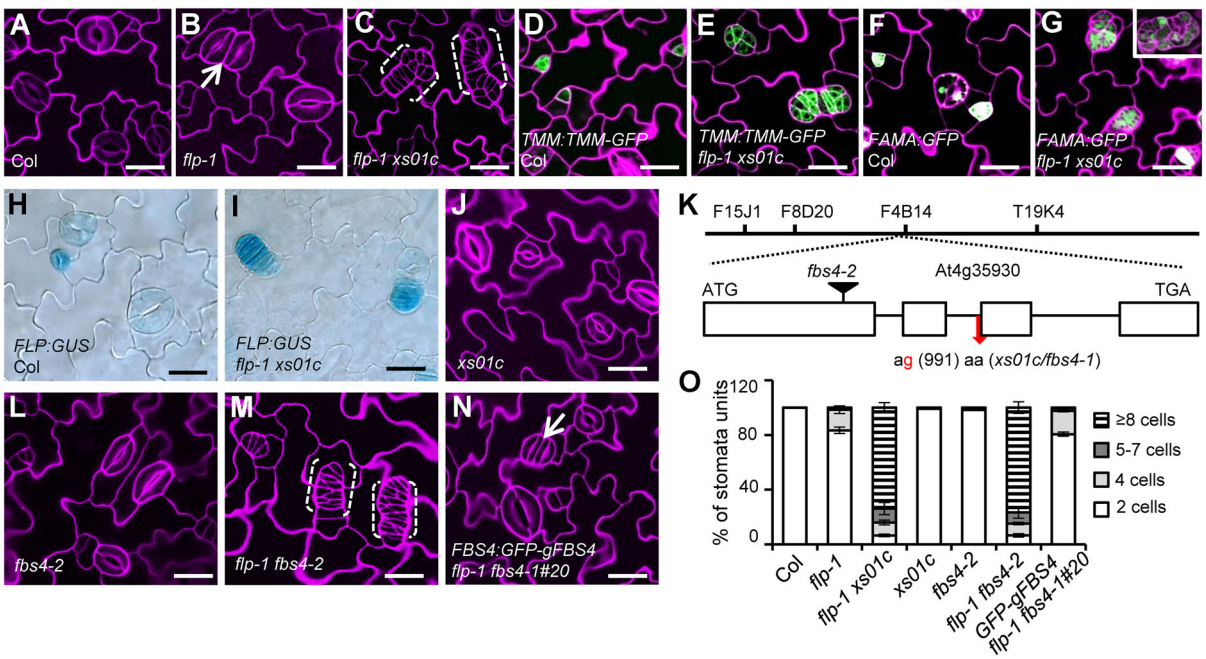

Figure 1. *XS01C* encodes the FBS4 protein that represses excessive stomatal division in the *Arabidopsis flp-1* mutant

(A) Normal 2-GC stomata in Col (wild type). Cell outlines were counterstained with propidium iodide but are presented in purple. **(B)** The white arrow indicates a 4-GC stomatal cluster in *flp-1*. **(C)** White brackets indicate the formation of large cell tumors in *flp-1 xs01c*. **(D)** Expression of the stomatal lineage marker *TMM:TMM-GFP* in a 6 d after plating (DAP) Col cotyledon. **(E)** Expression of *TMM:TMM-GFP* in the tumor cells of a 6-DAP *flp-1 xs01c* cotyledon. **(F)** *FAMA:GFP* expressed in GMCs and YGCs of an 8-DAP Col cotyledon. **(G)** Expression of *FAMA:GFP* in the tumor cells of an 8-DAP *flp-1 xs01c* cotyledon. Inset, *FAMA:GFP* expression in an enlarged tumor of a 13-DAP *flp-1 xs01c* cotyledon. **(H)** *FLP:GUS* expressed in GMCs and YGCs of a 6-DAP Col cotyledon. **(I)** *FLP:GUS* expression in the tumors of a 6-DAP *flp-1 xs01c* cotyledon. **(J)** No stomatal defect was found in the *xs01c* single mutant. **(K)** Map-based isolation and gene structure of the *XS01C/FBS4* gene. Boxes represent exons. The mutation site in *xs01c* is indicated by a red arrow, AG (991) changes to AA, which induces a splicing defect. A T-DNA insertion line, *fbs4-2*, is indicated by a triangle. **(L)** Normal stomata of the *fbs4-2* single mutant. **(M)** White brackets indicate the formation of giant cell tumors in the *flp-1 fbs4-2* double mutant. **(N)** Transformation with *FBS4:GFP-gFBS4* complements the over-dividing stomatal defects of *flp-1 fbs4-1*; transgenic line #20 is shown (see also Figure S4). An arrow indicates a *flp-1*-like 4-GC stomatal clusters. **(O)** Quantitative analysis of the cluster size from 8-DAP cotyledons. Data represent the means ± *SD*s (three individual experiments, $n = 25$). Scale bars, 20 μm. GC, guard cell; GMC, guard mother cell; YGC, young guard cell.

To obtain a single mutant, we crossed *flp-1 xs01c* with the wild type. The *xs01c* single mutant showed a normal stomatal phenotype, indicating that the formation of tumor-like cell clusters induced by the *xs01c* mutation is dependent on the *flp-1* mutant background (Figure 1J). *SPCH:SPCH-GFP* expression is transiently and specifically limited to stomatal lineage cells during the early stages of stomatal development (MacAlister et al., 2007). In the *flp-1 xs01c* epidermis, *SPCH:SPCH-GFP* expression was indistinguishable from that in wild-type plants, but it was absent in the stacked cells of tumors (Figure S1A, B). *MUTE:MUTE-GFP* is expressed in late Ms and early GMCs (Pillitteri et al., 2007). Interestingly, *MUTE:MUTE-GFP* expression was also present in some cells within the *flp-1 xs01c* tumors, indicating that these cells possess at least a GMC identity (Figure S1C, D). Occasionally, a few cells within a tumor eventually reached the mature GC stage, as assessed by the expression of the mature GC marker *E1728* (Figure S1E, F).

XS01C encodes FBS4 protein

To clone the *XS01C* gene, *flp-1 xs01c* was crossed with L*er* to generate a mapping population. Using a map-based cloning approach, we identified the mutation site of the *XS01C* gene in the approximately 17-kb interval between molecular markers F8D20 and T19K4 on chromosome IV (Figure 1K). After sequencing putative genes within this region of the *flp-1 xs01c* mutant, we found a G-to-A substitution at the splice donor site of the second intron of *FBS4* (At4g35930). Consequently, we renamed the homozygous mutant *xs01c* as *fbs4-1*. The mutation at the splicing site in *fbs4-1* produces two abnormal splicing variants that cause frameshift mutations, which probably lead to dysfunctional FBS4 proteins, although the tested transcription level in *fbs4-1* was higher than in wild type (Figure S2).

A homozygous mutant of SALK_032720C harboring a T-DNA insertion in the first exon of *FBS4* was named as *fbs4-2* (Figure 1K). As with *fbs4-1*, *fbs4-2* had a normal stomatal phenotype (Figure 1L). No significant changes in stomatal density or the stomatal index were found in *fbs4-1* and *fbs4-2* single mutants. However, we cannot exclude a possible role for *FBS4* in asymmetric divisions, similar to its *flp*-dependent role in symmetric division, that might be masked by other stomatal factors (Figure S3). The *flp-1 fbs4-2* double mutant displayed a stomatal defect similar to that of *flp-1 fbs4-1* (Figure 1M, O).

Furthermore, the introduction of genomic *FBS4* fused with GFP driven by the *FBS4* native promoter, *FBS4:GFP-gFBS4*, suppressed the formation of giant tumor-like cell clusters in *flp-1 fbs4-1*. For example, in a transgenic line #20, approximately 20% of stomata were in 4-GC clusters, and this resembled the stomatal phenotype of the *flp-1* single mutant (Figure 1N, O). Similar effects of the *FBS4:GFP-gFBS4* transgene on stomatal phenotype were observed in lines #25 and #60 (Figure S4A, B). Additionally, in *FBS4:GFP-gFBS4* transgenic line #41, which had a higher transgene

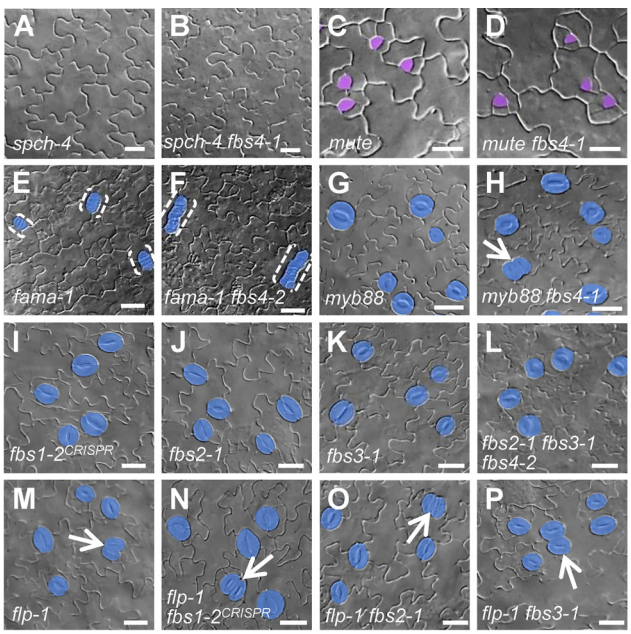

Figure 2. *FBS4* is specifically required to suppress excessive divisions in the *flp-1* mutant

(A, B) No stomata occurred on *spch-4* and *spch-4 fbs4-1* epidermal tissues. **(C, D)** Arrested meristemoids in *mute* and *mute fbs4-1* are highlighted in purple. **(E, F)** Enlarged cell tumors in the *fama-1 fbs4-2* double mutant in comparison with the *fama-1* single mutant. The cell tumors are highlighted in blue and brackets indicate the size. **(G, H)** In contrast to the normal stomata of *myb88, flp-1*-like stomatal clusters are occasionally found in the *myb88 fbs4-1* double mutant, as indicated by the white arrow. **(I–L)** The normal stomatal phenotypes of 8 d after plating (DAP) cotyledons from *fbs1-2*^{CRISPR}, *fbs2-1*, and *fbs3-1* single mutants, and the *fbs2-1 fbs3-1 fbs4-1* triple mutant. **(M–P)** Stomatal clusters of *flp-1 fbs1-2*^{CRISPR}, *flp-1 fbs2-1*, and *flp-1 fbs3-1* are indistinguishable from those of the *flp-1* single mutant. The white arrows indicate 4-GC stomatal clusters. GCs are highlighted in blue. Differential interference contrast microscopy images are of 8-DAP cotyledons. Scale bars, 20 μm. GC, guard cell.

expression level compared with the other lines, all the stomatal units were 2-GCs, suggesting that *FBS4* overexpression not only complements *flp-1 fbs4-1* tumor-like defects but also fully rescues *flp-1* stomatal defects (Figure S4C–E). In addition, both *flp-1 fbs4-1* and *flp-1 fbs4-2* double mutants exhibited dwarfed seedlings, delayed flowering time, and poor fertility, which were rescued by the transformation of genomic *FBS4*, suggesting that *FBS4* functions outside stomatal development (Figure S5).

The mutation of *FBS4* did not alter the stomatal phenotypes of *spch-4* and *mute* mutants, but it did enhance the tumor sizes in *fama-1* (Figure 2A–F). Although no stomatal defects were present in *myb88* and *fbs4-1* single mutants, *myb88 fbs4-1* occasionally displayed *flp-1*-like 4-GC stomatal clusters, in agreement with the functional redundancy of *FLP* and *MYB88* in GMC division (Figure 2G, H). We failed to obtain a *flp-1 myb88 fbs4-1* triple mutant, possibly because of the severe stomatal and plant growth defects. Thus, *FBS4* functions as a stage-specific repressor of excessive divisions at the terminal stage of stomatal development that are caused by a mutation of either *FLP*/*MYB88* or *FAMA*.

Evolutionary analysis of FBS proteins in plants

FBS4 contains four exons and encodes a 321-amino acid protein that is a member of the F-box protein family. Except for the F-box motif in the middle region of *FBS4*, no other recognizable domains were predicated by SWISS-MODEL. FBS4 has three paralogs in *Arabidopsis* that belong to the FBS subfamily of F-box proteins. FBS4 shares 15.26%, 16.82%, and 12.15% identity levels with FBS1, FBS2, and FBS3, respectively, and the F-box domain of FBS4 is well conserved, sharing 54.35%, 45.65%, and 41.30% identity levels, respectively. Proline85 (P85) within the F-box domain of FBS1 is a key residue for the interaction between FBS1 and the Arabidopsis Skp1-Like1 (ASK1) subunit of the SCF complex (Sepulveda-Garcia and Rocha-Sosa, 2012). A protein sequence alignment suggested that Proline166 (P166) of the FBS4 protein is a conserved residue possibly required for its interactions with ASKs of the SCF complex (Figure S6).

To characterize the possible roles of other FBS subfamily members in stomatal development, we examined the stomatal phenotypes in *fbs1-2*^{CRISPR} (a mutant obtained using clustered regularly interspaced palindromic repeats (CRISPR)/CRISPR-associated protein 9 (Cas9) technology), *fbs2-1* (SAIL_1187_G06), and *fbs3-1* (SALK_030006) (Figures 2I–K, S7). However, no stomatal defects were found in these single mutants, nor in the triple mutant *fbs2-1 fbs3-1 fbs4-1* (Figure 2L). Then, we crossed single mutants into the *flp-1* mutant background. Unlike *flp-1 fbs4-1*, neither *flp-1 fbs1-2*^{CRISPR}, *flp-1 fbs2-1*, nor *flp-1 fbs3-1* displayed cell tumors or an enhanced stomatal clustering phenotype, suggesting that FBS4 is specifically required to suppress excessive cell divisions in the *flp-1* mutant (Figure 2M–P).

The phylogenetic tree analysis indicated that in early land plants the appearance of FBS family homologs coincided with the appearance of stomata. For example, the unicellular green algae *Coccomyxa subellipsoidea* and *Chlamydomonas reinhardtii* have no FBS homologous genes in their genomes (Figure S8). However, moss and hornworst, the most ancient extant lineages to possess stomata, have putative FBS homologs (Chater et al., 2016, 2017). For example, four homologs are found in the model bryophyte *Physcomitrella patens*. Multiple homologs might exist in higher plants, such as the dicot plants *Glycine max* (8), *Solanum lycopersicum* (4), and *Medicago truncatula* (3), and the monocot plants *Zea mays* (8), *Sorghum bicolor* (2), *Oryza sativa* (2), and *Brachypodium distachyon* (3). All these proteins contain a typical F-box domain, which is a conserved sequence of approximately 50 amino acids (Maldonado-Calderon et al., 2012). The seagrass *Zostera marina* is a basal monocot that has re-adapted to a marine lifestyle, in which the absence of all the genes involved in stomatal differentiation has led to the loss of stomata (Olsen et al., 2016). However, *Z. marina* possesses three FBSs, suggesting that FBS proteins may have functions outside of stomatal development.

FBS4 plays a conserved function in stress responses

*FBS*s play roles in the general responses of plants to biotic and abiotic stresses (Maldonado-Calderon et al., 2012). However, whether *FBS4*, like the other *FBS* family members, is involved in stress responses remains unknown. In contrast to the hypersensitivity to salt stress displayed by *fbs2-1* and *fbs3-1*, *fbs4-1* displayed a sensitivity to salt similar to that of the wild type (Figure S9). FLP is a pleiotropic MYB transcription factor that is also involved in abiotic stress responses (Xie et al., 2010a). Compared with the wild type, the *flp-1* mutant displayed a hypersensitive response to a salt treatment, resulting a significantly reduced survival rate. Intriguingly, the *flp-1 fbs4-1* double mutant was more sensitive to salt stress than *flp-1*, which suggests that the function of FBS4 is closely linked to that of FLP outside of stomatal development (Figure S10A–I).

Jasmonates (JAs) are important phytohormones which mediate plant responses to abiotic and biotic stresses, including salt stress (Kazan, 2015). *FBS1* appears to be required for the modulation of JA-responsive genes (Gonzalez et al., 2017), and *JAZ10*, *VSP2*, and *PDF1.2* are immediate early, medium, and late JA-responsive genes, respectively (Lorenzo et al., 2004; Fernandez-Calvo et al., 2011). We analyzed changes in the transcriptional levels of these three genes at different time points after a 50 -μmol/L MeJA treatment. The JA-induced upregulation of *JAZ10* was greater in the *fbs4-1* mutant. However, the MeJA treatment did not induce *VSP2* expression in the *fbs4-1* mutant, and no significant change in *PDF1.2* expression was found between the wild type and *fbs4-1* (Figure S10J). The different, or even opposite, behaviors of JA-responsive genes may be associated with their distinct roles in different stress responses (Lorenzo et al., 2004; Fernandez-Calvo et al., 2011). Thus, it is very possible that FBS4 is involved in multiple JA-mediated stress responses.

FBS4 is expressed in stomatal precursor cells

The *Arabidopsis* eFP browser website database (http://bar.utoronto.ca/) indicated that *FBS4* is strongly expressed in stomatal lineage cells (Figure S11). Thus, we generated the *FBS4* native promoter-driven β-glucuronidase (GUS) reporter line *FBS4:GUS* to examine the *FBS4* expression pattern in *Arabidopsis*. In 5 d after plating (DAP) seedlings, *FBS4:GUS* was mainly expressed in veins and stomatal lineage cells in the epidermal tissues of cotyledons and leaves (Figure S12A–C), as well as in hypocotyls (Figure S12F). *FBS4:GUS* was also expressed in lateral root primordia and root tips (Figure S12D, E). However, in older 25-DAP seedlings, *FBS4:GUS* expression was not found in rosette leaves (Figure S12G). *FBS4:GUS* expression was also found in inflorescences and developing siliques but not in mature capsules (Figure S12H, I).

To further characterize the *FBS4* expression pattern within stomatal lineage cells, we compared the expression of *FBS4:GUS* with those of three stomatal stage-specific GUS reporters, *FLP:GUS-GFP*, *CDKB1;1:GUS*, and *CYCA2;3:GUS-GFP*. The expression of *FBS4:GUS* overlapped with those of the three reporter constructs in GMCs and YGCs. However, the *FBS4*-associated GUS activity was also detected in Ms at the early stage of stomatal development (Figure 3A, B). Furthermore, we analyzed the complementary transgenic line *FBS4:GFP-gFBS4*. However, the epidermal GFP florescent signals in all the tested transgenic plants were faint (Figure 3C). Consequently, we boosted the brightness of images taken from the green channel (Figure 3D). As shown in Figure 3E, GFP-gFBS4 was preferentially expressed in stomatal lineage cells from Ms and from GMCs to YGCs, but not in GCs (Figure 3E). In addition, the diffuse distribution of GFP-gFBS4 in stomatal precursor cells indicated that the FBS4 protein localized in both nuclei and cytoplasm (Figure S13).

Interactions with ASK via F-box domain affect FBS4's protein abundance

FBS4 is a protein containing a typical conserved F-box domain. Consequently, we determined whether this F-box domain was required for the interactions between FBS4 and the components of the SCF E3 ubiquitin ligase complex. Yeast two-hybrid assays showed that full-length FBS4 was able to interact with ASK1, a core component of the SCF complex (Cardozo and Pagano, 2004). However, a mutated FBS4$^{\Delta F\text{-box}}$, in which the F-box domain was deleted, failed to interact with ASK1. Additionally, FBS4$^{\Delta N}$ and FBS4$^{\Delta C}$, which lacked the N-terminus and C-terminus, respectively, but had intact F-box domains, maintained their interactions with ASK1. Furthermore, we substituted the Proline166 (P166) residue within the F-box domain of FBS4 with an alanine (P166A). FBS4^{P166A} displayed a reduced ability to interact with ASK1, which supported P166 being a functionally conserved residue in the

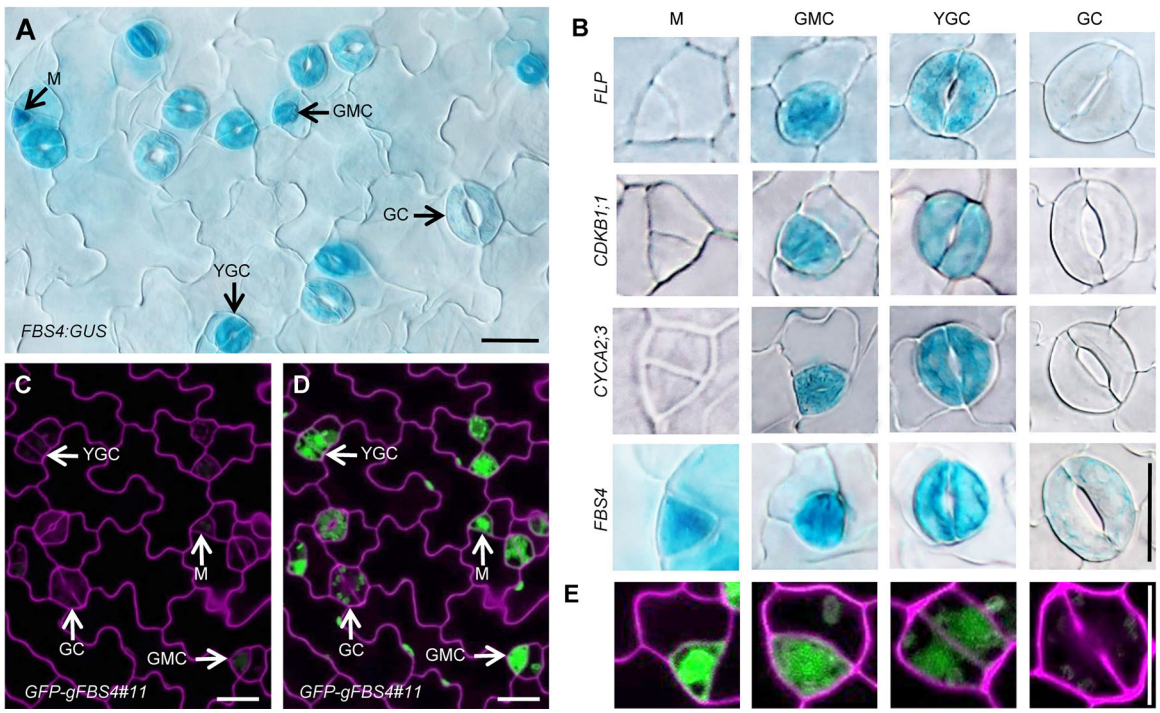

Figure 3. *FBS4* is specifically expressed within stomatal lineage cells in the epidermis

(A) Expression of *FBS4:GUS* in a developing 5 d after plating (DAP) cotyledon. **(B)** *FBS4:GUS* was strongly expressed in Ms, GMCs and YGCs, and its expression partially overlapped the expression of *FLP:GUS-GFP*, *CDKB1;1:GUS*, and *CYCA2;3:GUS* in GMCs and YGCs. **(C)** FBS4:GFP-gFBS4 fluorescence was very weak in the epidermis. **(D)** GFP-gFBS4 signals were boosted by adjusting image brightness. **(E)** Enlarged images of GFP-gFBS4 in stomatal lineage cells. FBS4 was localized in the nucleic and cytoplasm of Ms, GMCs, and YGCs but not of GCs. Scale bars, 20 μm. GC, guard cell; GMC, guard mother cell; M, meristemoid; YGC, young guard cell.

interactions between FBSs and ASKs (Sepulveda-Garcia and Rocha-Sosa, 2012) (Figure 4A). The interaction between FBS4 and ASK1 was verified using a luciferase complementation imaging (LCI) assay. However, the mutant FBS4$^{\Delta F\text{-box}}$ failed to interact with ASK1, confirming that the F-box domain is essential for the FBS4–ASK1 interaction (Figure S14B).

The application of MG132, an inhibitor that represses the activity of the 26S proteasome, enhanced the fluorescence signal of FBS4:GFP-gFBS4 (Figure 4B, C). To determine whether the assembly of FBS4 into the SCF complex was associated with its autocatalytic degradation, we separately introduced constructs carrying independent mutations of *FBS4*$^{\Delta F\text{-box}}$ and *FBS4*^{P166A} fused with GFP into *Arabidopsis*. Three transgenic lines harboring similar transcription levels of transgenes were confirmed by reverse-transcription quantitative polymerase chain reaction (RT-qPCR) analysis (Figure S15). Using the same imaging settings, we found that the GFP signal in FBS4:GFP-FBS4$^{\Delta F\text{-box}}$ was much stronger than that in FBS4:GFP-gFBS4. The intensity of the GFP signal in FBS4:GFP-FBS4^{P166A} was weaker than that in

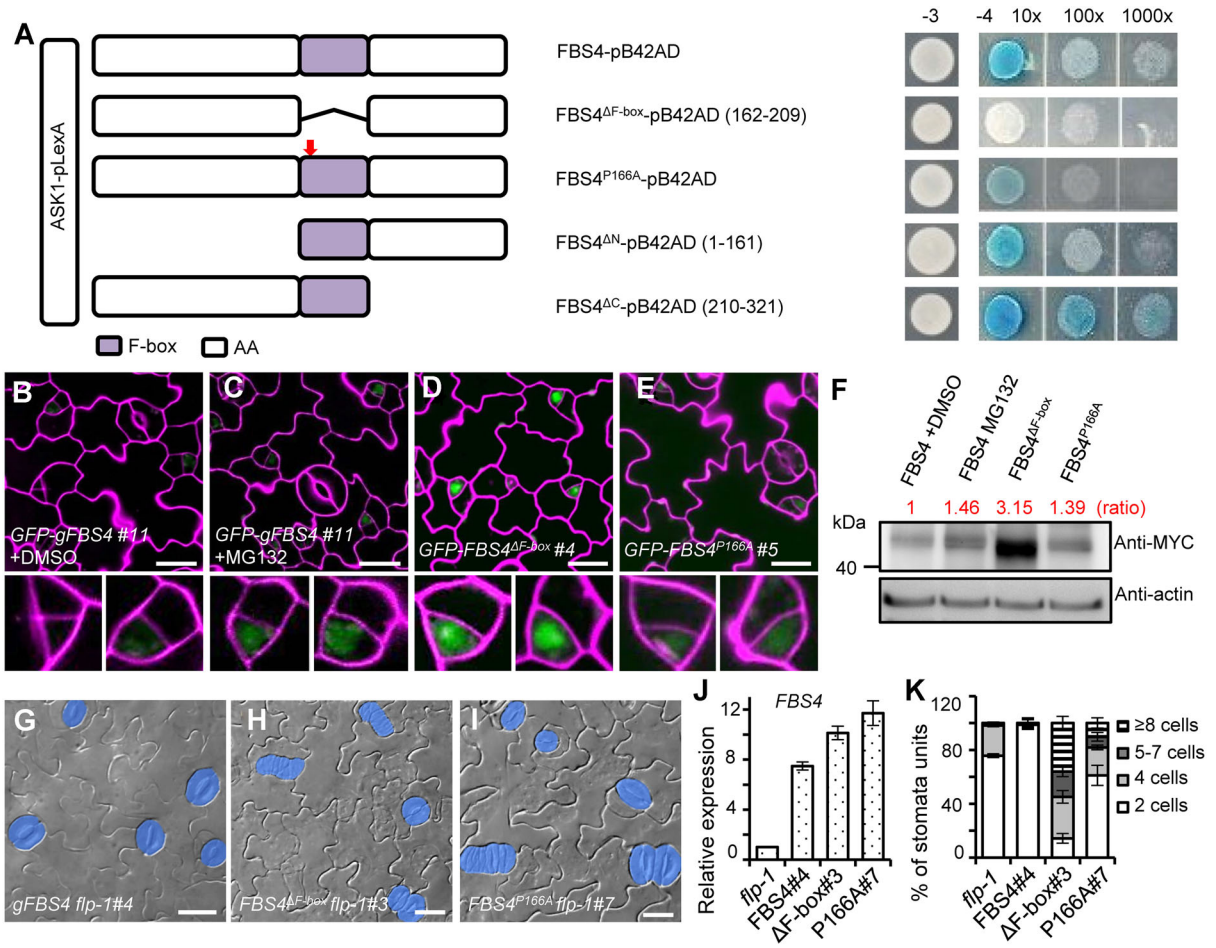

Figure 4. The F-box domain is essential for FBS4 function and the interaction with ASK1

(A) Yeast two-hybrid assays. The left diagram indicates the constructs used in the assay. The F-box domain is highlighted in purple. The red arrow indicates the position of the P166 residue. Transformants grown on the control media lacking His, Trp, and Ura (SD/-His/-Trp/-Ura, -3) and selective media lacking His, Leu, Trp, and Ura (SD/Gal/Raf/-His/-Leu/-Trp/-Ura, -4) at different dilutions (10×, 100×, and 1000×). Blue cones indicate positive interactions. The negative control is present in Figure S14A. **(B, C)** Green fluorescent protein (GFP) signals in 5 d after plating (DAP) *FBS4:GFP-gFBS4* epidermal tissues were barely detectable but enhanced after an 8-h MG132 (80 μmol/L) treatment. The panels underneath are enlarged images of Ms and GMCs. **(D, E)** By contrast, stronger GFP signals were present in precursor cells of *GFP-FBS4*$^{\Delta F\text{-box}}$ (F-box deletion variant) and *GFP-FBS4*^{P166A} (P166A substitution variant) transgenic plants. **(F)** FBS4 and variants fused with a MYC tag were transiently expressed in tobacco leaves and detected using western blotting. An MG132 treatment stabilized the FBS4 protein. Both FBS4$^{\Delta F\text{-box}}$ and FBS4^{P166A} displayed higher protein abundances compared with wild-type FBS4. Red numbers indicate relative ratios of protein levels relative to the wild-type FBS4 dimethyl sulfoxide mock after semi-quantification. Actin served as the loading control. **(G)** Overexpression of *FBS4* in *FBS4:gFBS4* line #4 rescued the stomatal cluster phenotype of *flp-1*. **(H, I)** Overexpression of *FBS4* variants of the F-box deletion in *FBS4:MYC-FBS4*$^{\Delta F\text{-box}}$ line #3 or P166A substitution in *FBS4:MYC-FBS4*^{P166A} line #7 aggravated the stomatal clustering phenotype of *flp-1*. **(J)** Overexpression levels of *FBS4* and variants were identified by RT-qPCR. Data are means ± *SD*s ($n = 12$). **(K)** Quantitative analysis of the cluster size from cotyledons of 8-DAP transgenic lines. Data represent the means ± *SD*s ($n = 25$). Scale bars, 20 μm. GMC, guard mother cell; RT-qPCR, reverse-transcription quantitative polymerase chain reaction.

FBS4:GFP-FBS4$^{\Delta F\text{-box}}$, but slightly greater than that in FBS4:GFP-gFBS4 (Figure 4B–E).

We failed to detect FBS4 proteins using a western blotting analysis in both GFP-gFBS4 and MYC-FBS4 transgenic plants, perhaps owing to the low abundance or short lifetime of the FBS4 protein in *Arabidopsis*. Next, we performed biochemical assays by transiently expressing *Arabidopsis FBS4* and its variants in *Nicotiana benthomiana* leaves (Figure 4F). Consistent with the observations in *Arabidopsis*, the application of MG132 increased the amount of FBS4 protein in tobacco leaves (relative ratio 1:1.46), indicating that the transiently expressed *Arabidopsis* FBS4 protein was degraded by tobacco 26S proteasomes. The amount of mutated MYC-FBS4$^{\Delta F\text{-box}}$ protein was approximately three times that of MYC-FBS4 (relative ratio 1:3.15). The mutation of P166A also caused an increase in the MYC-FBS4^{P166A} protein level compared with MYC-FBS4 (relative ratio 1:1.39). Consequently, we hypothesized that the deletion of the F-box domain or a point-mutation in P166A may disrupt the interactions between FBS4 and ASK1. The reduced assembly of F-box proteins into the SCF complex consequently decreases F-box degradation (Galan and Peter, 1999; Yu et al., 2015). Thus, the interaction of FBS4 with ASK1 via the F-box domain affects FBS4 protein abundance.

The F-box domain is critical for the FBS4-mediated repression of excessive cell division

Overexpressing FBS4 not only complemented the tumor-like phenotype of *flp-1 fbs4-1* but also rescued the 4-GC stomatal cluster defect caused by *flp-1* (Figure S4C—E). This result suggests that FBS4 may function downstream of FLP. We further verified the impact of *FBS4* overexpression on the *flp-1* single mutant. As shown in Figure 4G, only 2-GC stomata were found in *FBS4:gFBS4 flp-1* transgenic line #4 (Figure 4G, K). However, in *FBS4:gFBS4 flp-1* line #17, in which the *FBS4* transcript level is lower than in line #4, the effect of FBS4 on 4-GC stomatal cluster formation was limited (Figure S16). In contrast, overexpressing either *FBS4:MYC-FBS4*$^{\Delta F\text{-box}}$ or *FBS4:MYC-FBS4*^{P166A} in *flp-1* aggravated the stomatal clustering defect of the *flp-1* mutant, resulting in the production of larger clusters (Figure 4H–K). Thus, FBS4$^{\Delta F\text{-box}}$ and FBS4^{P166A} may compete with the endogenous FBS4 protein to interact with FBS4 substrates, but they are unable to mediate substrate degradation, leading to substrate accumulation (Yaron et al., 1998).

FBS4 genetically interacts with CYCA2-CDKB1 in stomatal terminal divisions

CYCA2;3 and CDKB1;1 are transcriptional targets of FLP/MYB88 during the terminal stage of stomatal development. We investigated whether CYCA2;3 and CDKB1;1 are the targeted substrates of FBS4-mediated post-translational regulation downstream of FLP. Because of the redundancy among *CYCA2* family members, the undivided GCs (SGCs) that were presented in higher order *cyca2* mutants were rarely found in the *cyca2* single mutant. No obvious stomatal defects were found in *cyca2;3* and *cyca2;3 fbs4-1*. However, the proportion of stomatal clusters was significantly reduced to 11.3% in the *cyca2;3 flp-1* double mutant in comparison with approximately 30% in the *flp-1* single mutant (Figure 5A–C, J). To further investigate the genetic relationships among *CYCA2;3*, *FLP*, and *FBS4*, we generated a *cyca2;3*^{CRISPR}*flp-1 fbs4-1* triple mutant using CRISPR/Cas9 technology (Figure S17). Compared with the giant tumors in *flp-1 fbs4-1*, the additional mutation of *CYCA2;3* led to reductions in the excessive cell proliferation of *flp-1 fbs4-1,* indicating that *CYCA2;3* functions downstream of *FLP* and *FBS4* (Figure 5D, E, J).

The stomatal defect of *cdkb1;1 1;2 flp-1* resembled that of *cdkb1;1 1;2* (Figure 5F, G). For example, 29.3% of stomata in *cdkb1;1 1;2* and 36.1% of stomata in *cdkb1;1 1;2 flp-1* were SGCs (Figure 5K). Surprisingly, no tumors or stomatal clusters were found in *cdkb1;1 1;2 flp-1 fbs4-1*, indicating that CDKB1 activities are required for the excessive divisions that occur in *flp-1 fbs4-1*. The loss of *FBS4* function significantly reduced the SGC proportion of the total stomata, resulting in 13.5% of SGCs in the *cdkb1;1 1;2 fbs4-1* triple mutant and 13.2% of SGCs in the *cdkb1;1 1;2 flp-1 fbs4-1* mutant, which indicated that the mutation of *FBS4* reduced the proportion of SGCs in *cdkb1;1 1;2* (Figure 5H, I, K). We previously reported that the formation of SGCs in a CDKB1;1 dominant negative line, *35:CDKB1;1.N161*, is rescued by *CYCA2;3*. CYCA2;3 overexpression results in a highly upregulated CDKA;1 transcription level, and its kinase activity may partially replace the CDKB1 function (Yang et al., 2014). It is plausible that, as a consequence of the increased CYCA2;3 level in *fbs4* mutants, the elevated CDKA;1 level is able to complement the GMC-division defects in the *cdkb1;1 1;2* mutant.

FBS4's function in stomatal division is independent of APC/C^{CCS52A1}

CCS52A1, as an activator of APC/C ubiquitin ligase, regulates the degradation of CYCA2;3 to control the endocycle onset. The stability of CYCA2;3-GFP is enhanced in *ccs52a1-1* mutant roots, indicating that CYCA2;3 is a CCS52A1 substrate (Boudolf et al., 2009). However, no stomatal division defect was found in the *ccs52a1-1* mutant. The stomatal clusters in *ccs52a1-1 flp-1* and *flp-1* were not discernable, suggesting that *CCS52A1*, unlike *FBS4*, may not be required for stomatal terminal division (Figure 5L). UVI4 is a specific inhibitor of APC/C^{CCS52A1}, and CYCA2;3 fails to accumulate in the *uvi4* mutant (Heyman et al., 2011). Consistently, the mutation of *UVI4* had no influence on the defective divisions in *flp-1* and *flp-1 fbs4-1* (Figure 5M). Thus, the APC/C^{CCS52A1} complex may not participate in stomatal development. However, SCF^{FBS4} plays an important role in repressing excessive divisions at the terminal stage of stomatal development.

FBS4 is physically associated with the CYCA2;3 protein

To determine whether FBS4 associates with the CDKB1;1-CYCA2;3 complex and regulates its stability, we first

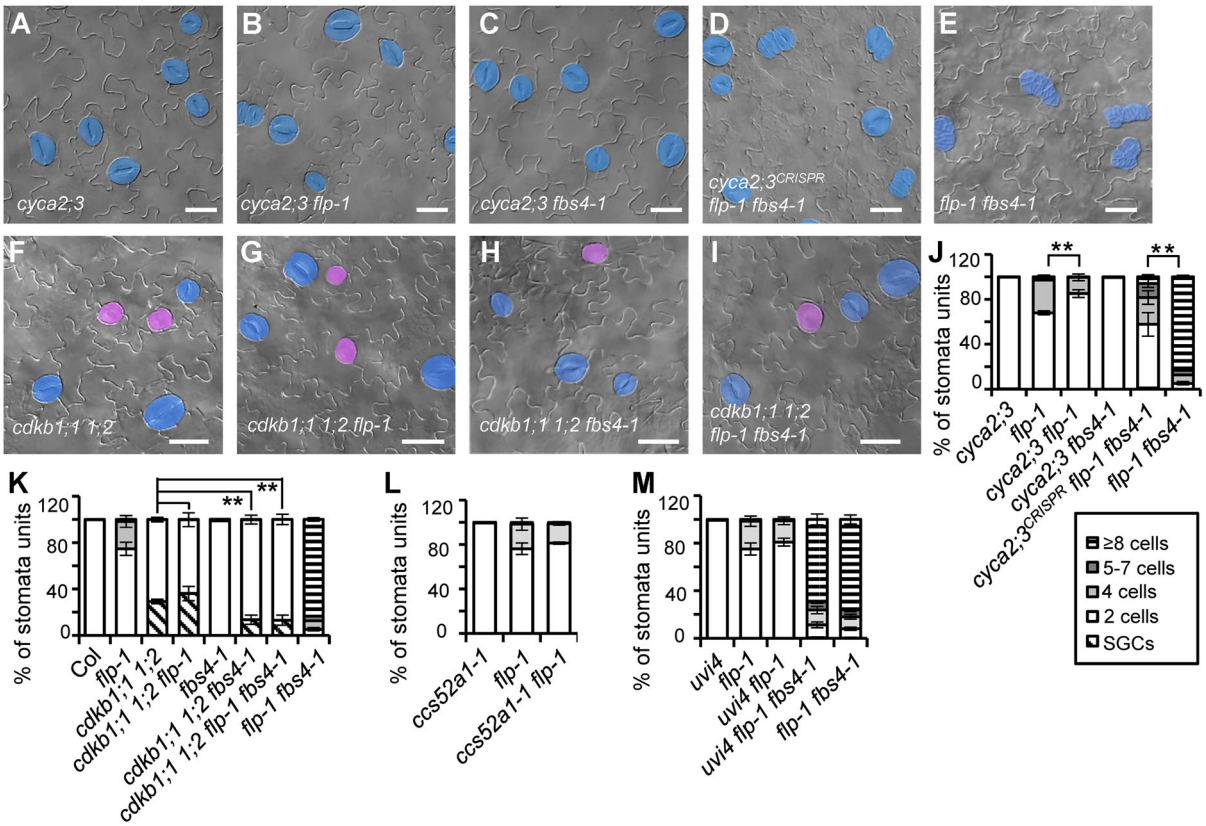

Figure 5. FBS4 functions in stomatal terminal division through CYCA2-CDKB1

(A–C) Mutation in *cyca2;3* partially suppressed stomatal clusters in *flp-1* but had no impact on *fbs4-1*. **(D, E)** Loss of the *CYCA2;3* function in *cyca2;3*^{CRISPR} significantly reduced the stomatal cluster size of *flp-1 fbs4-1*. Quantitative analysis of cell numbers in stomatal units of **(A–E)**, see panel **(J)**. **(F, G)** The mutation of *flp-1* did not change the SGC proportion in *cdkb1;1 1;2*. *cdkb1;1 1;2* fully suppressed the stomatal cluster formation caused by *flp-1*. **(H)** *fbs4-1* reduced the proportion of SGCs in *cdkb1;1 1;2*. **(I)** *flp-1 fsb4-1* partially suppressed the formation of SGCs in *cdkb1;1 1;2*, whereas *cdkb1;1 1;2* fully suppressed the stomatal cluster formation caused by *flp-1 fbs4-1*. Quantitative analysis of stomatal units of **(F–I)**, see panel **(K)**. SGCs are highlighted in red. GCs and stomatal clusters are highlighted in blue. **(L)** Stomata are normal in *ccs52a1-1* mutants. The mutation of *ccs52a1-1* had no impact on the *flp-1* stomatal clustering phenotype. **(M)** The *uvi4* mutant had normal stomata. The mutation of *uvi4* had no impact on the excessive divisions in *flp-1* and *flp-1 fbs4-1*. **(J–M)** Quantitative analysis of stomatal phenotypes from 8 d after plating (DAP) cotyledons. Data represent the means ± *SD*s (n = 25). Asterisks indicate significant differences (Student's *t*-test, $^{**}P < 0.01$). Scale bars in **(A–I)**, 20 μm. GC, guard cell; SGC, single guard cell.

performed yeast two-hybrid assays. However, no interactions were found between full-length FBS4 and either CYCA2;3, CDKB1;1 or the dominant negative form CDKB1;1.N161. Surprisingly, the F-box deletion variant FBS4$^{\Delta F\text{-box}}$ interacted with CYCA2;3 but not with CDKB1;1 or CDKB1;1.N161 (Figure 6A). We then performed a co-immunoprecipitation analysis to confirm these results. *MYC-FBS4*$^{\Delta F\text{-box}}$ was co-expressed with *CYCA2;3-GFP* or negative control *GFP* alone in *Nicotiana benthamiana* leaves. Total proteins were isolated and incubated with GFP agarose beads to immunoprecipitate CYCA2;3-GFP and GFP proteins. As shown in Figure 6B, MYC-FBS4$^{\Delta F\text{-box}}$ was detected with precipitated CYCA2;3-GFP but not with GFP alone (Figure 6B). Furthermore, we performed bimolecular fluorescence complementation experiments. Strong yellow fluorescent protein (YFP) signals were observed in epidermal cells of *Nicotiana benthamiana* leaves co-transformed with *nYFP-FBS4*$^{\Delta F\text{-box}}$ and *cYFP-CYCA2;3*, confirming a physical interaction between FBS4 and CYCA2;3 (Figure 6C).

FBS4 promotes CYCA2;3 degradation via the ubiquitination–26S proteasome pathway

Although the transcription of *CYCA2;3* was upregulated in *flp-1*, both *fbs4-1* and *flp-1 fbs4-1* displayed CYCA2;3 transcript levels similar to that of the wild type (Figure 6D). To determine whether CYCA2;3 is regulated by FBS4 at the protein level, we first investigated the CYCA2;3-GFP protein using seedlings expressing the *XVE:CYCA2;3-GFP* fusion protein (Imai et al., 2006; Boudolf et al., 2009). Although dramatically increased GFP signals were present in roots after the MG132 treatment, no detectable GFP expression was observed in the leaf epidermis (Figure S18). Therefore, we infiltrated *CYCA2;3-GFP* into *Nicotiana benthamiana* leaves and detected the CYCA2;3-GFP protein by western blotting. The MG132 treatment increased the accumulation of CYCA2;3-GFP, indicating that the transiently expressed *Arabidopsis* CYCA2;3-GFP protein was degraded by tobacco 26S proteasomes (Figure 6E). To verify the effects of FBS4 on the CYCA2;3 protein, we co-expressed *CYCA2;3-GFP* with

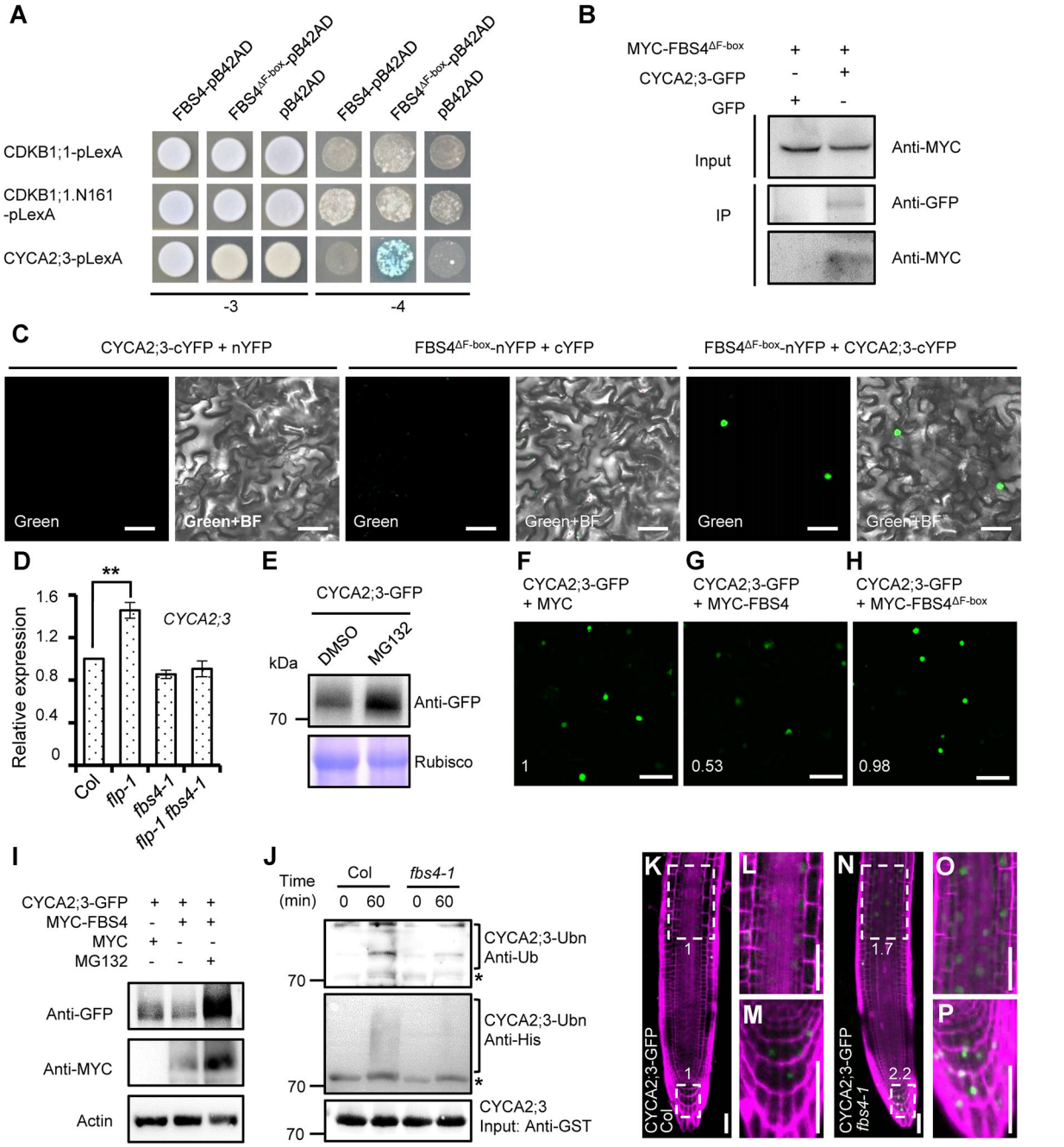

Figure 6. FBS4 targets the CYCA2;3 protein for degradation

(A) FBS4$^{\Delta F\text{-box}}$ interacted with CYCA2;3 in a yeast two-hybrid assay. Transformants grown on the control media (SD/-His/-Trp/-Ura, -3) and selective media (SD/Gal/Raf/-His/-Leu/-Trp/-Ura, -4). Blue indicates positive interactions. **(B)** FBS4$^{\Delta F\text{-box}}$ associated with CYCA2;3 in a co-immunoprecipitation assay. **(C)** The bimolecular fluorescence complementation assay demonstrated an interaction between FBS4$^{\Delta F\text{-box}}$ and CYCA2;3. Green, yellow fluorescent protein (YFP) signals indicated a positive interaction. BF, bright-field image. **(D)** RT-qPCR analysis of *CYCA2;3* transcription in 10 d after plating (DAP) seedlings. Asterisks indicate significant differences compared with Col wild type (Student's *t*-test, $^{**}P < 0.01$). Data are means ± *SD*s of three biological replicates ($n = 12$). **(E)** MG132 stabilized transiently expressed *Arabidopsis* CYCA2;3-GFP (green fluorescent protein) in *Nicotiana benthamiana* leaves. Coomassie Brilliant Blue (CCB) staining; rubisco served as the loading control. **(F–H)** Transient co-expression with MYB-FBS4 reduced the CYCA2;3-GFP intensity. GFP fluorescence in the epidermis was detected 3 d after infiltration. The numbers in the lower left corners indicate the GFP intensities relative to CYCA2;3 co-expressed with MYC (see also Figure S19). **(I)** The FBS4-promoted degradation of CYCA2;3-GFP was inhibited by MG132. **(J)** Analysis of CYCA2;3 ubiquitination in protein extracts prepared from GST-CYCA2;3-transformed Col and *fbs4-1* seedlings. Brackets indicate uibiquitinated CYCA2;3 proteins. Asterisks indicate GST-CYCA2;3 proteins. **(K–P)** Confocal images of induced *XVE:CYCA2;3-GFP* in Col and *fbs4-1* mutant roots. Five DAP seedlings were induced with 50 μmol/L β-estradiol for 16 h before imaging. L, M, O, and P, enlarged images of the regions denoted in K and N. Numbers next to the white boxes represent the fluorescence intensities in the measured areas (see also Figure S20). Scale bars, 20 μm **(C, F–H)** and 50 μm **(K–P)**. RT-qPCR, reverse-transcription quantitative polymerase chain reaction.

MYC, *MYC-FBS4* and *MYC-FBS4*$^{\Delta F\text{-}box}$ independently in *Nicotiana benthamiana* leaves. The intensity of CYCA2;3-GFP signals were noticeably reduced in leaves co-expressing MYC-FBS4 relative to those co-expressing MYC and MYC-FBS4$^{\Delta F\text{-}box}$ (Figure 6F–H). A quantitative analysis of the relative GFP intensity in nuclei revealed that the CYCA2;3-GFP intensity was reduced by approximately 50% when co-expressed with MYC-FBS4, compared with the MYC control. By contrast, co-expressing CYCA2;3-GFP with FBS4$^{\Delta F\text{-}box}$ had no impact on the CYCA2;3-GFP intensity (Figure S19). Furthermore, the application of MG132 greatly inhibited FBS4-induced CYCA2;3-GFP degradation (Figure 6I).

To determine whether FBS4 mediated the ubiquitination of CYCA2;3 *in vivo*, we investigated the GST-CYCA2;3 ubiquitination status in wild-type and *fbs4-1* protein extracts. The GST-CYCA2;3 was polyubiquitinated in the wild-type protein extracts but was less ubiquitinated in the *fbs4-1* extracts (Figure 6J). The ubiquitination of CYCA2;3 in *fbs4-1* mutant did not absolutely disappear. This may be because other E3 ligases ubiquitinated the CYCA2;3 protein. Thus, FBS4 can mediate CYCA2;3 ubiquitination. Interestingly, the intensity of the nuclear localized CYCA2;3-GFP signals in *fbs4-1* roots, especially in columella and elongation-zone cells, was stronger than in the wild-type background, indicating that a similar FBS4 regulatory effect on CYCA2;3 stability might exist during root development (Figures 6K–P, S20). In conclusion, our results demonstrate that FBS4 degrades the CYCA2;3 protein through ubiquitin-proteasome pathways.

DISCUSSION

E3 ubiquitin ligase-mediated protein degradation plays important roles in many processes, such as auxin signaling, organ development, and stress responses (Wang et al., 2016; Zhu et al., 2017). CONSTITUTIVE PHOTOMORPHOGENIC1, a ring finger ligase, mediates stomatal development by targeting SCREAM/ICE1 proteins for degradation (Lee et al., 2017). FBL17 forms an SCF protein—E3 ubiquitin ligase complex (SCF^{FBL17}) that targets the cyclin-dependent kinase inhibitors KRP6 and KRP7 for proteasome-dependent degradation (Kim et al., 2008). The invalidation of F-box protein FBL17 induces an increase in stomatal density (Noir et al., 2015). However, F-box proteins and ubiquitin ligase complex-mediated protein modifications involved in regulating the late stage of stomatal development have not been fully studied. Here, we identified and characterized the functional role of the F-box protein FBS4 in repressing excessive terminal divisions during stomatal development. FBS4 physically interacted with CYCA2;3 and induced its degradation via the ubiquitin-26S proteasome pathway. Malfunctions in SCF^{FBS4} complex-mediated CYCA2;3 degradation in the *flp-1* mutant CYCA2;3 induced cell overproliferation during the terminal division, resulting in the formation of giant tumor-like cell clusters in the epidermis (Figure 7).

FBS4 belongs to the four-member FBS subfamily in *Arabidopsis*. *FBS1* is rapidly induced by biotic and abiotic stresses, and FBS1 regulates multiple genes that respond to the plant stress hormones JA and abscisic acid (Gonzalez et al., 2017). Here, we demonstrated that FBS4 has a conserved function in the regulation of JA-responsive genes. However, unlike other FBS subfamily member mutants, the *fbs4* mutant displayed a *flp-1* background hypersensitivity to salt stress, suggesting that the function of FBS4 in stress responses is closely associated with that of FLP.

The F-box domain is important for FBS1 interactions with ASK1. A mutation of Proline85 (P85A) suppresses the FBS1 interaction with ASK1 (Maldonado-Calderon et al., 2012; Sepulveda-Garcia and Rocha-Sosa, 2012). Proline166 within the FBS4 F-box domain plays a conserved function in the interaction of FBS4 with ASK1. Deleting the intact F-box domain or substituting the key residue P166A interrupted the assembly of FBS4 into SCF ligase complexes, resulting in an increase in FBS4 protein stability.

SCFs target substrates for degradation, and F-box proteins in SCF complexes specifically mediate interactions with substrates (Sullivan et al., 2003). Most F-box proteins are predicted to use specific C-terminal domains to recognize substrates, such as leucine-rich regions, WD-40, and Kelch repeats. However, there is a large number of F-box proteins in *Arabidopsis* that do not contain a consensus C-terminal domain (Gagne et al., 2002). According to an analysis of SMART and PFAM data, FBS4 has no representative domain within its C-terminus, suggesting that FBS4 may use novel domains to interact with specific targets.

FLP, MYB88, and FAMA are involved in the repression of the transcription of core cell-cycle genes, including *CYCA2;3* and *CDKB1;1*, ensuring that the terminal division happens only once (Lai et al., 2005; Xie et al., 2010a; Vanneste et al., 2011). We speculated that FBS4, as a F-box protein, regulates these core cell-cycle genes at post-translational level. A genetic analysis revealed that the *cyca2;3* mutant partly rescued the cluster phenotype of *flp-1 fbs4-1*, demonstrating that *cyca2;3* is epistatic to *fbs4-1* with respect to stomatal terminal division. The decreased proportions of undivided SGCs in *cdkb1;1 1;2 fbs4-1* and *cdkb1;1 1;2 flp-1 fbs4-1* were consistent with the roles of CYCA2s in regulating CDKB1 activity during the stomatal GMC division.

CYCA2;3 and CDKB1;1 can form complexes to determine the timing of the mitosis-to-endocycle transition. CCS52A1 and UVI4 function as activator and inhibitor of APC/C complexes, respectively, to regulate CYCA2;3 stability, control endocycle onset, and affect cell proliferation (Boudolf et al., 2009; Heyman et al., 2011). However, the additional mutation of *CCS52A1* or *UVI4* had no influence on the stomatal defects of *flp-1* and *flp-1 fbs4-1* (Figure 5L, M). In addition, we used flow cytometry to detect DNA ploidy levels in wild-type and *fbs4-1* cotyledons, and no obvious differences were detected (Figure S21), indicating that FBS4 may act within stomatal lineage cells by suppressing cell overproliferation.

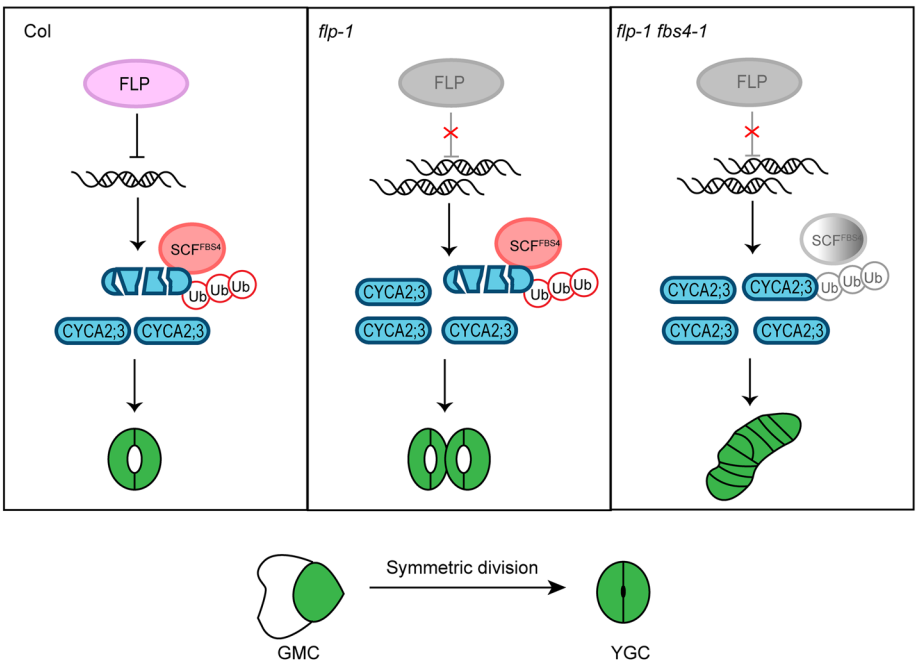

Figure 7. FBS4 is involved in suppressing the excessive terminal divisions of stomatal development
FOUR LIPS (FLP) was involved in the repression of the transcription of core cell-cycle genes, including CYCA2;3, ensuring that the terminal division occurred only once. FBS4 interacted with ASK1 and promoted CYCA2;3 degradation via the ubiquitination-26S proteasome pathway. Malfunctions of SCF^{FBS4} complex-mediated CYCA2;3 degradation in the *flp-1* mutant induced cell overproliferation during the terminal division, resulting in the formation of giant tumor-like cell clusters in the epidermis.

In addition to being expressed in stomatal lineages of the epidermis, *FBS4:GUS* was also expressed in root tips (Figure S12E), and CYCA2;3 stability increased in *fbs4* roots (Figure 6N–P). *UVI4* regulates endocycle onset in leaves as well as maintaining root meristem size. The mutation of *UVI4* causes a decrease in the number of meristematic cortex cells, resulting in a smaller root meristem size compared with the wild type (Hase et al., 2006; Heyman et al., 2011). Thus, we compared the lengths of root meristematic zones in different mutant combinations. The mutation of *FBS4* had no significant impact on the root meristematic length, either in *flp-1, uvi4*, or *uvi4 flp-1* mutant backgrounds, suggesting that UVI4-mediated CYCA2;3 stability is the major regulatory pathway in roots (Figure S22), which indicates distinct roles for $APC/C^{CCS52A1}$ and SCF^{FBS4} in plant development.

MATERIALS AND METHODS

Plant materials and growth conditions

Arabidopsis thaliana Columbia (Col-0) was used as the wild type in all experiments. Mutant seeds of *fbs2-1* (SAIL_1187_G06), *fbs3-1* (SALK_030006) and *fbs4-2* (SALK_032720C) were obtained from the Arabidopsis Biological Resource Center (ABRC). The following mutants *flp-1* (Lai et al., 2005), *cdkb1;1 1;2* (Xie et al., 2010a), *cyca2;3* (Vanneste et al., 2011), *ccs52a1-1* (Xu et al., 2016), *uvi4* (Iwata et al., 2011), *spch-4* (MacAlister et al., 2007), *mute* (Pillitteri et al., 2007) and *fama-1* (Ohashi-Ito and Bergmann, 2006) were used. The following transgenic seeds *FLP:GUS-GFP* (Lai et al., 2005), *CDKB1;1:GUS* (Xie et al., 2010a), *CYCA2;3:GUS-GFP* (Vanneste et al., 2011) were used. The *cyca2;3 flp-1*, *cyca2;3 fbs4-1*, *cdkb1;1 1;2 flp-1 fbs4-1*, *cdkb1;1 1;2 flp-1*, *cdkb1;1 1;2 fbs4-1*, *uiv4 flp-1*, *uvi4 flp-1 fbs4-1*, *ccs52a1-1 flp-1* were generated by cross and PCR-based approaches. *FBS4:GFP-gFBS4 flp-1 fbs4-1*, *FBS4:GFP-gFBS4* Col, *FBS4:GFP-FBS4*$^{\Delta F\text{-}box}$ Col, *FBS4:GFP-FBS4*^{P166A} Col, *FBS4:MYC-FBS4*$^{\Delta F\text{-}box}$ *flp-1*, *FBS4:MYC-FBS4*^{P166A} *flp-1* and *FBS4:gFBS4 flp-1* were generated by the floral-dip method (Clough and Bent, 1998). *Arabidopsis* plants were grown on half-strength Murashige and Skoog (MS) medium containing 1% sucrose at 22 °C under 16 h/8 h light/dark cycles.

Map-based cloning

The screened method in the *flp-1* background has been described previously (Yang et al., 2019). To clone the *XS01C* gene, the *flp-1 xs01c* was crossed with L*er* and generated F2 mapping populations. The plants having tumor cells in cotyledon were selected for mapping by using *Arabidopsis* molecular markers which were developed from an *Arabidopsis* mapping platform (http://amp.genomics.org.cn/). The *XS01C* mutation was finely mapped to a region and then putative genes within this region were sequenced (BGI Company).

Constructs and plant transformation

To obtain *FBS4:GFP-gFBS4, FBS4:GFP-FBS4*$^{\Delta F\text{-}box}$ and *FBS4:GFP-FBS4*^{P166A} constructs, the 2945-bp promoter of *FBS4* was amplified using the primers ProFBS4-p1300221-F and ProFBS4-p1300221-R. The genomic fragment *gFBS4* was amplified with primers gFBS4-F and gFBS4-R. GFP-F and GFP-R were used to amplify *GFP*. Above fragments were subcloned into a *pCAMBIA1300* vector by one-step method. The sequences of primers are listed in Table S1. The mutated *FBS4*^{P166A} DNA fragment was generated by 496 bp C to G site-directed mutagenesis of *FBS4* fragment. For transient expression in *N. benthamiana*, the GFP- or MYC-fused *FBS4*, *FBS4*$^{\Delta F\text{-}box}$, *CYCA2;3* sequences were cloned into the *pSUPER1300* vector (Ni et al., 1995; Yang et al., 2010). The *cyca2;3*^{CRISPR}*flp-1 fbs4-1* triple mutant and *fbs1-2*^{CRISPR} were generated by CRISPR/Cas9 technology as previously described (Xing et al., 2014). Briefly, the guide RNAs (gRNAs) were designed to target the second exon of *CYCA2;3* and F-box domain of *FBS1*. Then the gRNAs were cloned into the *pHEE041* vector. The constructs were electroporated into *Agrobacteria tumefaciens* EHA105 and transformed into *flp-1 fbs4-1* double mutant and Col, respectively. Transgenic plants were selected on half-strength MS medium supplemented with 30 μg/L hygromycin.

GUS staining

Four-d-old *FBS4:GUS* cotyledons were incubated in 90% acetone for 1 h at 4 °C. After washing in phosphate buffer for three times, cotyledons were stained in enzymatic reaction solution (Wang et al., 2015) and incubated at 37 °C for 2 h. Ethanol:Acetic acid (3:1) solution was used to remove chlorophyll after GUS staining.

Real-time quantitative PCR

Total RNA was isolated from different organs using HiPure Plant RNA Mini Kit (http://www.magentec.com). The first-strand complementary DNA (cDNA) was synthesized by the Promega Reverse-Transcription Kit (http://www.promega.com) according to the manufacturer's instructions. RT-qPCR was performed with Hieff qPCR SYBR Green Master Mix (Yeason) on a Roche Light cycler 96. We calculated the ratios by using $2^{-\Delta\Delta C_t}$. Three biological replicates were conducted in all experiments. For the expression level of *FBS4*, *ACTIN2* gene was used as the control. For the expression level of *JAZ10* (1 h treatment), *VSP2* (8 h treatment) and *PDF1.2* (24 h treatment), total RNA of 7-d-old Col and *fbs4-1* seedlings were extracted at 1, 8, 24 h after 50 μmol/L MeJA treatment. The *ACTIN8* gene was used as the internal control. Primer sequences are list in Table S1.

Yeast two-hybrid assay

The yeast two-hybrid assay method was previously described (Song et al., 2011). The cDNA of *FBS4* was amplified with primers in Table S1 and cloned into the vector *pB42AD* (Clontech). *ASK1* was cloned into vector *pLexA* (Clontech). The two vectors were co-transformed into yeast strain EGY48 [p8op-lacZ] and plated on SD/-His/-Trp/-Ura DO supplement (Clontech) at 30 °C for 3–4 d. Then the yeast transformants were selected on 2% Gal/1% raffinose/SD/-Ura/-His/-Trp/-Leu/X-β-Gal. The interactions were observed after 3–7 d of incubation at 22 °C.

Bimolecular fluorescence complementation assay

The cDNA sequences of *CYCA2;3* and *FBS4*$^{\Delta F\text{-}box}$ were cloned into the *pSPYNE-35S* and *pSPYCE-35S*, respectively. *CYCA2;3-CE* and *FBS4*$^{\Delta F\text{-}box}$*-NE* were transformed into EHA105. *Agrobacterium* strains carrying the paired constructs together with the p19 strain were injected into *Nicotiana benthomiana* leaves. The YFP signal was observed at the 3rd d after infiltration using a confocal scanning microscope (Olympus FV1000MPE). Leaves were injected with a solution containing 40 μmol/L MG132 (Sigma-Aldrich) 12 h before observation (Kim et al., 2019).

Co-immunoprecipitation assay

To examine the interaction of FBS4$^{\Delta F\text{-}box}$ and CYCA2;3 *in planta*, the constructs were infiltrated into 4-week-old *Nicotiana benthamiana*. A solution containing 80 μmol/L MG132 was injected into the leaf tissues 12 h before collection (Kim et al., 2019). Total proteins were extracted with extraction buffer (Boudolf et al., 2009) supplemented with 80 μmol/L MG132 and protease inhibitor cocktail (Roche). Antibodies for anti-MYC mAb-Agarose (MBL) were added to the protein extracts (1.5 mg) and incubated for 1 h at 4 °C. The beads were washed with wash buffer (50 mmol/L Tris-HCl, 150 mmol/L NaCl, 5 mmol/L ethyleneglycotetraacetic acid, and 1 mmol/L dithiothreitol, pH 7.6) five times. The protein samples were separated in 10% sodium dodecyl-sulfate (SDS)-polyacrylamide gel and detected by immunoblot analysis with anti-MYC (MBL) and anti-GFP (MBL) antibodies, respectively.

Luciferase complementation imaging assays

Luciferase complementation imaging assays were performed as described previously (Chen et al., 2008). Each fragment of *FBS4*, *FBS4*$^{\Delta F\text{-}box}$, and *ASK1* were amplified by PCR using the primer pairs of FBS4-cluc-F and FBS4-cluc-R or ASK1-nluc-F and ASK1-nluc-R which are listed in Table S1. Fragments were cloned into the *pCAMBIA-NLuc* or *pCAMBIA-CLuc* vectors. FBS4-CLuc or FBS4$^{\Delta F\text{-}box}$-CLuc and ASK1-Nluc were co-expressed in *N. benthamiana* leaves. Two days after infiltration, the leaves were treated with 40 μmol/L MG132 (Sigma-Aldrich) for 12 h before observation (Kim et al., 2019).

Transient expression analysis

The transient expression assays were performed in *Nicotiana benthamiana* leaves. The coding sequences of *FBS4*, *FBS4*$^{\Delta F\text{-}box}$, *FBS4*^{P166A}, and *CYCA2;3* fused with *GFP* or *MYC* tag sequence were cloned into a modified *pCAMBIA1300* vector (CAMBIA) driven by *SUPER* promoter. Different combinations were co-transformed into 4-week-old *Nicotiana benthamiana*. Infected leaves were observed under a confocal laser scanning microscope (Olympus) after 3 d. All experiments were repeated three times with similar results. The relative fluorescence intensities were measured using ImageJ software (http://imagej.nih.gov/ij/). For the western blotting protein

analysis, Rubisco or actin (antibody β-actin, CWBIO, CW0264M) served as loading controls.

In vitro ubiquitination assay

The *CYCA2;3* was cloned into *pGEX4T-1* vector and transformed into BL21 strain of *Escherichia coli*. The transformed strains were grown to 600 nm optical density = 0.5 at 37°C and then were induced with 0.4 mmol/L isopropyl-β-D-1-thiogalactopyranoside (IPTG) at 16 °C for 15 h. Phosphate-buffered saline (PBS) was used as buffer to lyse the harvested strains. The GST-CYCA2;3 protein was enriched by glutathione-Sepharose (GE Healthcare) and divided into four groups.

Total protein was extracted from 4-d-old seedlings of Col and *fbs4-1* with extraction buffer. Each reaction included 100 μL GST-CYCA2;3, 2 μg UBQ-His, 2 mmol/L adenosine triphosphate, 80 μmol/L MG132, and 600 μg Col/*fbs4-1* supernatant for 0 and 60 min. After reaction, the protein samples were loaded on the 8% SDS-polyacrylamide gel, followed by western blotting using anti-GST (MBL), anti-His (MBL), and anti-ubiquitin (Sigma-Aldrich).

ACKNOWLEDGEMENTS

We thank Dominique Bergmann for SPCH:SPCH-GFP, MUTE:MUTE-GFP markers, Yunhai Li for *ccs52a1-1* and *uvi4 Arabidopsis* seeds, Qijun Chen for *pHEE401* and *pCBC-DT1T2* vectors, Lieven De Veylder for *XVE:CYCA2;3-GFP* seeds, Jianmin Zhou for *pCAMBIA-NLuc* and *pCAMBIA-CLuc* vectors. We thank Jingquan Li and Suhua Yang from Plant Science Facility of the Institute of Botany, Chinese Academy of Sciences for their excellent technical assistances. This work was supported by grants from the National Natural Science Foundation of China to J.L. (31771515 and 31970804) and to K.Y. (31871377 and 32070723).

CONFLICT OF INTEREST

The authors declare they have no competing interests.

AUTHOR CONTRIBUTIONS

Y.L., K.Y., and J.L. designed research. S.X. provided the *flp-1 xs01c* mutant. Y.L., Q.H., L.L.Z., J.X.W., Z.B.F., and J.Z. performed research. Y.L., C.R.Z., and J.L.Y. analyzed data. Y.L., C.X.Z., J.J.Z., and J.L. wrote the manuscript. All authors read and approved of its content.

Edited by: Juan Dong, Rutgers the State University of New Jersey, USA

Received Aug. 21, 2021; **Accepted** Nov. 21, 2021; **Published** Nov. 24, 2021

REFERENCES

Abd-Hamid, N.A., Ahmad-Fauzi, M.I., Zainal, Z., and Ismail, I. (2020). Diverse and dynamic roles of F-box proteins in plant biology. Planta **251:** 68.

Ban, Z., and Estelle, M. (2021). CUL3 E3 ligases in plant development and environmental response. Nat. Plants **7:** 6–16.

Boudolf, V., Lammens, T., Boruc, J., Van Leene, J., Van Den Daele, H., Maes, S., Van Isterdael, G., Russinova, E., Kondorosi, E., Witters, E., De Jaeger, G., Inze, D., and De Veylder, L. (2009). CDKB1;1 forms a functional complex with CYCA2;3 to suppress endocycle onset. Plant Physiol. **150:** 1482–1493.

Cardozo, T., and Pagano, M. (2004). The SCF ubiquitin ligase: Insights into a molecular machine. Nat. Rev. Mol. Cell Biol. **5:** 739–751.

Casson, S.A., and Hetherington, A.M. (2010). Environmental regulation of stomatal development. Curr. Opin. Plant Biol. **13:** 90–95.

Chater, C.C., Caine, R.S., Tomek, M., Wallace, S., Kamisugi, Y., Cuming, A.C., Lang, D., MacAlister, C.A., Casson, S., Bergmann, D. C., Decker, E.L., Frank, W., Gray, J.E., Fleming, A., Reski, R., and Beerling, D.J. (2016). Origin and function of stomata in the moss *Physcomitrella patens*. Nat. Plants **2:** 16179.

Chater, C.C.C., Caine, R.S., Fleming, A.J., and Gray, J.E. (2017). Origins and evolution of stomatal development. Plant Physiol. **174:** 624–638.

Chen, H., Zou, Y., Shang, Y., Lin, H., Wang, Y., Cai, R., Tang, X., and Zhou, J.M. (2008). Firefly luciferase complementation imaging assay for protein-protein interactions in plants. Plant Physiol. **146:** 368–376.

Chen, Q., Liu, Y., Maere, S., Lee, E., Van Isterdael, G., Xie, Z., Xuan, W., Lucas, J., Vassileva, V., Kitakura, S., Marhavy, P., Wabnik, K., Geldner, N., Benkova, E., Le, J., Fukaki, H., Grotewold, E., Li, C., Friml, J., Sack, F., Beeckman, T., and Vanneste, S. (2015). A coherent transcriptional feed-forward motif model for mediating auxin-sensitive PIN3 expression during lateral root development. Nat. Commun. **6:** 8821.

Clough, S.J., and Bent, A.F. (1998). Floral dip: A simplified method for Agrobacterium-mediated transformation of *Arabidopsis thaliana*. Plant J. **16:** 735–743.

den Elzen, N., and Pines, J. (2001). Cyclin A is destroyed in prometaphase and can delay chromosome alignment and anaphase. J. Cell Biol. **153:** 121–136.

Fang, S., and Weissman, A.M. (2004). A field guide to ubiquitylation. Cell. Mol. Life Sci. **61:** 1546–1561.

Fernandez-Calvo, P., Chini, A., Fernandez-Barbero, G., Chico, J.M., Gimenez-Ibanez, S., Geerinck, J., Eeckhout, D., Schweizer, F., Godoy, M., Franco-Zorrilla, J.M., Pauwels, L., Witters, E., Puga, M.I., Paz-Ares, J., Goossens, A., Reymond, P., De Jaeger, G., and Solano, R. (2011). The *Arabidopsis* bHLH transcription factors MYC3 and MYC4 are targets of JAZ repressors and act additively with MYC2 in the activation of jasmonate responses. Plant Cell **23:** 701–715.

Gagne, J.M., Downes, B.P., Shiu, S.H., Durski, A.M., and Vierstra, R.D. (2002). The F-box subunit of the SCF E3 complex is encoded by a diverse superfamily of genes in *Arabidopsis*. Proc. Natl. Acad. Sci. U.S. A. **99:** 11519–11524.

Galan, J.M., and Peter, M. (1999). Ubiquitin-dependent degradation of multiple F-box proteins by an autocatalytic mechanism. Proc. Natl. Acad. Sci. U.S.A. **96:** 9124–9129.

Geley, S., Kramer, E., Gieffers, C., Gannon, J., Peters, J.M., and Hunt, T. (2001). Anaphase-promoting complex/cyclosome–dependent proteolysis of human cyclin A starts at the beginning of mitosis and is not subject to the spindle assembly checkpoint. J. Cell Biol. **153:** 137–148.

Gonzalez, L.E., Keller, K., Chan, K.X., Gessel, M.M., and Thines, B.C. (2017). Transcriptome analysis uncovers *Arabidopsis* F-BOX STRESS INDUCED 1 as a regulator of jasmonic acid and abscisic acid stress gene expression. BMC Genomics **18:** 533.

Guo, L., Jiang, L., Zhang, Y., Lu, X.L., Xie, Q., Weijers, D., and Liu, C.M. (2016). The anaphase-promoting complex initiates zygote division in *Arabidopsis* through degradation of cyclin B1. Plant J. **86:** 161–174.

Hase, Y., Trung, K.H., Matsunaga, T., and Tanaka, A. (2006). A mutation in the *uvi4* gene promotes progression of endo-reduplication and confers increased tolerance towards ultraviolet B light. Plant J. **46:** 317–326.

Hautbergue, G., and Goguel, V. (1999). The yeast C-type cyclin Ctk2p is phosphorylated and rapidly degraded by the ubiquitin-proteasome pathway. Mol. Cell. Biol. **19:** 2527–2534.

Heyman, J., Polyn, S., Eekhout, T., and De Veylder, L. (2017). Tissue-specific control of the endocycle by the anaphase promoting complex/cyclosome Inhibitors UVI4 and DEL1. Plant Physiol. **175:** 303–313.

Heyman, J., Van den Daele, H., De Wit, K., Boudolf, V., Berckmans, B., Verkest, A., Alvim Kamei, C.L., De Jaeger, G., Koncz, C., and De Veylder, L. (2011). *Arabidopsis* ULTRAVIOLET-B-INSENSITIVE4 maintains cell division activity by temporal inhibition of the anaphase-promoting complex/cyclosome. Plant Cell **23:** 4394–4410.

Hua, Z., and Vierstra, R.D. (2011). The cullin-RING ubiquitin-protein ligases. Annu. Rev. Plant Biol. **62:** 299–334.

Imai, K.K., Ohashi, Y., Tsuge, T., Yoshizumi, T., Matsui, M., Oka, A., and Aoyama, T. (2006). The A-type cyclin CYCA2;3 is a key regulator of ploidy levels in *Arabidopsis* endoreduplication. Plant Cell **18:** 382–396.

Iwata, E., Ikeda, S., Matsunaga, S., Kurata, M., Yoshioka, Y., Criqui, M. C., Genschik, P., and Ito, M. (2011). GIGAS CELL1, a novel negative regulator of the anaphase-promoting complex/cyclosome, is required for proper mitotic progression and cell fate determination in *Arabidopsis*. Plant Cell **23:** 4382–4393.

Jackson, L.P., Reed, S.I., and Haase, S.B. (2006). Distinct mechanisms control the stability of the related S-phase cyclins Clb5 and Clb6. Mol. Cell. Biol. **26:** 2456–2466.

Kazan, K. (2015). Diverse roles of jasmonates and ethylene in abiotic stress tolerance. Trends Plant Sci. **20:** 219–229.

Kim, H., Yu, S.I., Jung, S.H., Lee, B.H., and Suh, M.C. (2019). The F-Box protein SAGL1 and ECERIFERUM3 regulate cuticular wax biosynthesis in response to changes in humidity in *Arabidopsis*. Plant Cell **31:** 2223–2240.

Kim, H.J., Oh, S.A., Brownfield, L., Hong, S.H., Ryu, H., Hwang, I., Twell, D., and Nam, H.G. (2008). Control of plant germline proliferation by SCF (FBL17) degradation of cell cycle inhibitors. Nature **455:** 1134–1137.

Lai, L.B., Nadeau, J.A., Lucas, J., Lee, E.K., Nakagawa, T., Zhao, L., Geisler, M., and Sack, F.D. (2005). The *Arabidopsis* R2R3 MYB proteins FOUR LIPS and MYB88 restrict divisions late in the stomatal cell lineage. Plant Cell **17:** 2754–2767.

Lee, J.H., Jung, J.H., and Park, C.M. (2017). Light inhibits COP1-mediated degradation of ICE transcription factors to induce stomatal development in *Arabidopsis*. Plant Cell **29:** 2817–2830.

Lorenzo, O., Chico, J.M., Sanchez-Serrano, J.J., and Solano, R. (2004). *JASMONATE-INSENSITIVE1* encodes a MYC transcription factor essential to discriminate between different jasmonate-regulated defense responses in *Arabidopsis*. Plant Cell **16:** 1938–1950.

MacAlister, C.A., Ohashi-Ito, K., and Bergmann, D.C. (2007). Transcription factor control of asymmetric cell divisions that establish the stomatal lineage. Nature **445:** 537–540.

Makkena, S., Lee, E., Sack, F.D., and Lamb, R.S. (2012). The R2R3 MYB transcription factors FOUR LIPS and MYB88 regulate female reproductive development. J. Exp. Bot. **63:** 5545–5558.

Maldonado-Calderon, M.T., Sepulveda-Garcia, E., and Rocha-Sosa, M. (2012). Characterization of novel F-box proteins in plants induced by biotic and abiotic stress. Plant Sci. **185-186:** 208–217.

Nadeau, J.A., and Sack, F.D. (2002). Control of stomatal distribution on the *Arabidopsis* leaf surface. Science **296:** 1697–1700.

Nakayama, K.I., and Nakayama, K. (2005). Regulation of the cell cycle by SCF-type ubiquitin ligases. Semin. Cell Dev. Biol. **16:** 323–333.

Ni, M., Cui, D., Einstein, J., Narasimhulu, S., Vergara, C.E., and Gelvin, S.B. (1995). Strength and tissue-specificity of chimeric promoters derived from the octopine and mannopine synthase genes. Plant J. **7:** 661–676.

Noir, S., Marrocco, K., Masoud, K., Thomann, A., Gusti, A., Bitrian, M., Schnittger, A., and Genschik, P. (2015). The control of *Arabidopsis thaliana* growth by cell proliferation and endoreplication requires the F-Box protein FBL17. Plant Cell **27:** 1461–1476.

Ohashi-Ito, K., and Bergmann, D.C. (2006). *Arabidopsis* FAMA controls the final proliferation/differentiation switch during stomatal development. Plant Cell **18:** 2493–2505.

Olsen, J.L., Rouze, P., Verhelst, B., Lin, Y.C., Bayer, T., Collen, J., Dattolo, E., De Paoli, E., Dittami, S., Maumus, F., Michel, G., Kersting, A., Lauritano, C., Lohaus, R., Topel, M., Tonon, T., Vanneste, K., Amirebrahimi, M., Brakel, J., Bostrom, C., Chovatia, M., Grimwood, J., Jenkins, J.W., Jueterbock, A., Mraz, A., Stam, W.T., Tice, H., Bornberg-Bauer, E., Green, P.J., Pearson, G.A., Procaccini, G., Duarte, C.M., Schmutz, J., Reusch, T.B., and Van de Peer, Y. (2016). The genome of the seagrass *Zostera marina* reveals angiosperm adaptation to the sea. Nature **530:** 331–335.

Pillitteri, L.J., Sloan, D.B., Bogenschutz, N.L., and Torii, K.U. (2007). Termination of asymmetric cell division and differentiation of stomata. Nature **445:** 501–505.

Pillitteri, L.J., and Torii, K.U. (2012). Mechanisms of stomatal development. Annu. Rev. Plant Biol. **63:** 591–614.

Sepulveda-Garcia, E., and Rocha-Sosa, M. (2012). The *Arabidopsis* F-box protein AtFBS1 interacts with 14-3-3 proteins. Plant Sci. **195:** 36–47.

Song, S., Qi, T., Huang, H., Ren, Q., Wu, D., Chang, C., Peng, W., Liu, Y., Peng, J., and Xie, D. (2011). The Jasmonate-ZIM domain proteins interact with the R2R3-MYB transcription factors MYB21 and MYB24 to affect Jasmonate-regulated stamen development in *Arabidopsis*. Plant Cell **23:** 1000–1013.

Sullivan, J.A., Shirasu, K., and Deng, X.W. (2003). The diverse roles of ubiquitin and the 26S proteasome in the life of plants. Nat. Rev. Genet. **4:** 948–958.

Vanneste, S., Coppens, F., Lee, E., Donner, T.J., Xie, Z., Van Isterdael, G., Dhondt, S., De Winter, F., De Rybel, B., Vuylsteke, M., De Veylder, L., Friml, J., Inze, D., Grotewold, E., Scarpella, E., Sack, F., Beemster, G.T., and Beeckman, T. (2011). Developmental regulation of CYCA2s contributes to tissue-specific proliferation in *Arabidopsis*. EMBO J. **30:** 3430–3441.

Wang, H.Z., Yang, K.Z., Zou, J.J., Zhu, L.L., Xie, Z.D., Morita, M.T., Tasaka, M., Friml, J., Grotewold, E., Beeckman, T., Vanneste, S., Sack, F., and Le, J. (2015). Transcriptional regulation of PIN genes by FOUR LIPS and MYB88 during *Arabidopsis* root gravitropism. Nat. Commun. **6:** 8822.

Wang, Z., Li, N., Jiang, S., Gonzalez, N., Huang, X., Wang, Y., Inze, D., and Li, Y. (2016). SCF(SAP) controls organ size by targeting PPD proteins for degradation in *Arabidopsis thaliana*. Nat. Commun. **7:** 11192.

Willems, A., Heyman, J., Eekhout, T., Achon, I., Pedroza-Garcia, J.A., Zhu, T., Li, L., Vercauteren, I., Van den Daele, H., van de Cotte, B., De Smet, I., and De Veylder, L. (2020). The cyclin CYCA3;4 is a postprophase target of the APC/C(CCS52A2) E3-ligase controlling formative cell divisions in *Arabidopsis*. Plant Cell **32:** 2979–2996.

Wu, S.Y., Kuan, V.J., Tzeng, Y.W., Schuyler, S.C., and Juang, Y.L. (2016). The anaphase-promoting complex works together with the SCF complex for proteolysis of the S-phase cyclin Clb6 during the transition from G1 to S phase. Fungal Genet. Biol. **91:** 6–19.

Xie, Z., Lee, E., Lucas, J.R., Morohashi, K., Li, D., Murray, J.A., Sack, F. D., and Grotewold, E. (2010a). Regulation of cell proliferation in the stomatal lineage by the *Arabidopsis* MYB FOUR LIPS via direct targeting of core cell cycle genes. Plant Cell **22:** 2306–2321.

Xie, Z., Li, D., Wang, L., Sack, F.D., and Grotewold, E. (2010b). Role of the stomatal development regulators FLP/MYB88 in abiotic stress responses. Plant J. **64:** 731–739.

Xing, H.L., Dong, L., Wang, Z.P., Zhang, H.Y., Han, C.Y., Liu, B., Wang, X.C., and Chen, Q.J. (2014). A CRISPR-Cas9 toolkit for multiplex genome editing in plants. BMC Plant Biol. **14:** 327.

Xu, Y., Jin, W., Li, N., Zhang, W., Liu, C., Li, C., and Li, Y. (2016). UBIQUITIN-SPECIFIC PROTEASE14 interacts with ULTRAVIOLET-B INSENSITIVE4 to regulate endoreduplication and cell and organ growth in *Arabidopsis*. Plant Cell **28:** 1200–1214.

Yang, H., Shi, Y., Liu, J., Guo, L., Zhang, X., and Yang, S. (2010). A mutant CHS3 protein with TIR-NB-LRR-LIM domains modulates growth, cell death and freezing tolerance in a temperature-dependent manner in *Arabidopsis*. Plant J. **63:** 283–296.

Yang, K.Z., Wang, H.Z., Xue, S., Qu, X.X., Zou, J.J., and Le, J. (2014). Requirement for A-type cyclin-dependent kinase and cyclins for the terminal division in the stomatal lineage of *Arabidopsis*. J. Exp. Bot. **65:** 2449–2461.

Yang, K.Z., Zhu, L.L., Wang, H.Z., Jiang, M., Xiao, C.W., Hu, X.Y., Vanneste, S., Dong, J., and Le, J. (2019). A conserved but plant-specific CDK-mediated regulation of DNA replication protein A2 in the precise control of stomatal terminal division. Proc. Natl. Acad. Sci. U.S.A. **116:** 18126–18131.

Yaron, A., Hatzubai, A., Davis, M., Lavon, I., Amit, S., Manning, A.M., Andersen, J.S., Mann, M., Mercurio, F., and Ben-Neriah, Y. (1998). Identification of the receptor component of the IkappaBalpha-ubiquitin ligase. Nature **396:** 590–594.

Yoshida, A., Choi, J., Jin, H.R., Li, Y., Bajpai, S., Qie, S., and Diehl, J.A. (2021). Fbxl8 suppresses lymphoma growth and hematopoietic transformation through degradation of cyclin D3. Oncogene **40:** 292–306.

Yu, H., Zhang, Y., Moss, B.L., Bargmann, B.O., Wang, R., Prigge, M., Nemhauser, J.L., and Estelle, M. (2015). Untethering the TIR1 auxin receptor from the SCF complex increases its stability and inhibits auxin response. Nat. Plants **1:** 14030.

Zhu, J.Y., Li, Y., Cao, D.M., Yang, H., Oh, E., Bi, Y., Zhu, S., and Wang, Z.Y. (2017). The F-box protein KIB1 mediates brassinosteroid-induced inactivation and degradation of GSK3-like kinases in *Arabidopsis*. Mol. Cell **66:** 648–657.

SUPPORTING INFORMATION

Additional Supporting Information may be found online in the supporting information tab for this article: http://onlinelibrary.wiley.com/doi/10.1111/jipb.13193/suppinfo

Figure S1. Expression patterns of stomatal lineage markers in wild-type and *flp-1 xs01c* mutant cotyledons

(**A, B**) *SPCH:SPCH-GFP* expression patterns are similar between Col and *flp-1 xs01c* (2 d after plating (DAP)). (**C**, **D**) Expression of GMC marker *MUTE:MUTE-GFP* can be found in the cells within the tumors of *flp-1 xs01c* (3 DAP). (**E, F**) Expression of *E1728* indicates the mature GCs that occasionally formed within the tumors of *flp-1 xs01c* (8 DAP). Scale bars, 20 μm. GC, guard cell; GMC, guard mother cell.

Figure S2. The mutation in *FBS4* splicing site leads to reading frame shifts

(**A**) The point-mutation in the second intron of *FBS4* results in two different splice variants. The first wrong cut (*FBS4-WC-1*), 588 bp–601 bp of *FBS4* complementary DNA sequence is deleted. The second intron (*FBS4-WC-2*), is not spliced successfully. Two splice variants all lead to frame shift mutation. (**B**) The gene expression levels of *FBS4* in *fbs4-1* higher than Col; primers are shown by red arrows (**A**). Asterisks indicate significant differences relative to Col (Student's *t*-test, ** $P < 0.01$). Data are means ± *SD* ($n = 15$).

Figure S3. No significant changes on stomatal density and index in *fbs4-1* and *fbs4-2* mutants

(**A**) The stomatal densities (**B**) The stomatal indexes. Data are represented as means ± *SD* ($n = 25$). No significant differences in comparison with Col after Student's *t*-test.

Figure S4. Transformation of *FBS4* gene complements the stomatal defects in *flp-1 fbs4-1* mutants

(**A, B**) In *FBS4:GFP-gFBS4* transgenic lines #25 and #60, transformation of genomic *FBS4* partially complements the stomatal clustering phenotype in *flp-1 fbs4-1*. (**C**) In transgenic line #41, *FBS4* fully complements the stomatal defects of *flp-1 fbs4-1* to normal. Stomatal GCs are highlighted with blue color. Scale bars, 20 μm. (**D**) The transcriptional level of *FBS4* in transgenic line #41 is much higher than other lines, corresponding to its stronger complementary effect on stomatal defects. The stomatal phenotype of Line #21 is shown in Figure 1N. (**E**) Quantitative analysis of the cluster size. Data represent the mean ± *SD* ($n = 25$). GC, guard cell.

Figure S5. Additional mutation of *FBS4* causes retarded plant growth in *flp-1* mutant background

(**A**) The side-views of 30-d-old plants. Addition mutation of *FBS4*, either by *fbs4-1* or by *fbs4-2*, caused a retarded plant growth and delayed flowering in *flp-1* mutants. Transformation of *FBS4:GFP-gFBS4* restored the plant growth of *flp-1 fbs4-1* (transgenic line#20). (**B**) Top views of same seedlings shown in panel (**A**). Scale bar, 2 cm.

Figure S6. The sequence alignments of F-BOX STRESS-INDUCED (FBS) family genes and proteins

(**A**) Alignment of *FBS1*, *FBS2*, *FBS3*, *FBS4* complementary DNA sequences. Black underline indicates the region encoding F-BOX domain. (**B**) Alignment of amino acid sequences of FBS family proteins. Black underline indicates the F-box domain, in which P85 of FBS1 and P166 of FBS4 (indicated by red asterisks) are conserved residues for their interaction with Arabidopsis Skp1-Like1 (ASK1) of Skp1/Cullin/F-box (SCF) complex.

Figure S7. Generation and identification of *FBS* family mutants

(**A**) *fbs1-2*^{CRISPR} was created by clustered regularly interspaced palindromic repeats (CRISPR)/CRISPR-associated protein 9 (Cas9)-based genome editing. Protospacer adjacent motif sequence is labeled in green color. (**B**) Identification of T-DNA insertion lines *fbs2-1* and *fbs3-1*. Primers used in reverse-transcription – polymerase chain reaction (RT-PCR) are indicated by red arrows.

Figure S8. Phylogenetic relationships of F-BOX STRESS-INDUCED (FBS) proteins in plants

Phylogenetic tree was constructed using amino acid sequences by the neighbor-joining method of MEGA7. Bootstrap values for 1 000 replicates are given in nodes as percent. *Arabidopsis thaliana*, *Zea mays*, *Brachypodium distachyon*, *Glycine max*, *Oryza sativa*, *Physcomitrella patens*, *Zostera marina*, *Medicago truncatula*, *Sorghum bicolor*, *Solanum lycopersicum*. Underlined letters used for the species abbreviations.

Figure S9. *fbs2* and *fbs3* mutants are hypersensitive to salt stress

(**A**–**F**) Compared to Col, both *fbs2-1* and *fbs3-1* mutants display hypersensitive response to salt stress. Top-view images of 20-d-old seedlings after 6 d treatment with 300 mmol/L NaCl. (**G, H**) *fbs4-1* displays a similar sensitivity to salt stress with Col. (**I**) Quantitative analysis of seedling survival rate. Data represent the mean ± *SD* (3 individual experiments, $n = 64$); Statistical analysis, $P < 0.05$, Duncan's multiple range test.

Figure S10. F-BOX STRESS-INDUCED 4 (FBS4) is involved salt stress and jasmonate (JA)-responsive gene expression

(**A**–**H**) Top-view images of 20-d-old seedlings after 6 d of 300 mmol/L NaCl treatment. Compared to Col or *fbs4-1*, *flp-1* displays a sensitive response to salt stress, while *flp-1 fbs4- 1* seedlings are hypersensitive to salt stress. (**I**) Quantitative analysis of the survival rates. Data represent the mean ± *SD* (3 individual experiments, $n = 64$). The specific differences in means were compared with Duncan's multiple range test ($P < 0.05$). (**J**) Real-time quantitative polymerase chain reaction (PCR) analysis shows the relative expression changes of 3 JA-responsive genes after 50 μmol/L MeJA treatment in 8 d after plating plants, *JAZ10* (at 1 h), *VSP2* (at 8 h), and *PDF1.2* (at 24 h). The messenger RNA levels were normalized to *ACTIN8*. Data represent the mean ± *SD* (repeated from three biological experiments, $n = 12$). Asterisks indicate significant difference to Col (Student's *t*-test, **$P < 0.01$, *$P < 0.05$).

Figure S11. *FBS4* is predicated on having a preferential expression profile within stomatal lineage cells
The results obtained from *Arabidopsis* eFP browser website (http://bar.utoronto.ca/).
Figure S12. Expression pattern of *FBS4:GUS* reporter in *Arabidopsis*
(**A**) *FBS4:GUS* expression in a 5 d after plating (DAP) seedling. (**B**) β-glucuronidase (GUS) expression in veins and epidermis of cotyledon. (**C**) Preferential expression of *FBS4:GUS* in stomatal lineage cells in cotyledon epidermis. (**D**) GUS expression in a lateral root primordium. (**E**) GUS expression in a primary root tip. (**F**) GUS expression in vein and stomata in a hypocotyl. (**G**) No GUS signal is found in a 25-DAP rosette leaf. (**H**) GUS in 25-DAP inflorescence and young siliques. (**I**) No GUS expression in a mature capsule. Scale bars, 2 mm (**A, G, H, I**), 200 μm (**B**), 50 μm (**D, E**), and 20 μm (**C, F**).
Figure S13. Subcellular localization of F-BOX STRESS-INDUCED 4 (FBS4) in stomatal precursors
(**A**) Confocal images of epidermis of FBS4:GFP-gFBS4 cotyledons. Cell outlines are counterstained with propidium iodide but presented in purple color. Due to the weak expression of green fluorescent protein (GFP)-gFBS4, image brightness of GFP channel was upregulated before merging. *xy* view, a single optical section from confocal z-stacks. *yz* view and *xz* view, the orthogonal views along the yellow crossline. (**B**) The enlarged three-dimensional images of the region within the white box are shown in panel (**A**). GFP signals are enriched in the cytoplasm and the nucleus of a stomatal precursor. Scale bars, 20 μm (**A**), 5 μm (**B**).
Figure S14. F-box domain mediates F-BOX STRESS-INDUCED 4 (FBS4) interaction with Arabidopsis Skp1-Like1 (ASK1)
(**A**) Negative control for yeast two-hybrid assay shown in Figure 4A. Transformants grown on the control media lacking His, Trp, and Ura (SD/-His/-Trp/-Ura, -3) and selective media lacking His, Leu, Trp, and Ura (SD/Gal/Raf/-His/-Leu/-Trp/-Ura, -4) with different dilution times (10×, 100×, and 1000×). (**B**) The interaction between FBS4 and ASK1 was verified as well by a luciferase complementation imaging (LCI) assay. However, mutated FBS4$^{\Delta F\text{-}box}$ failed to interact with ASK1, confirming that the F-box domain is essential for the FBS4-ASK1 interaction.
Figure S15. The *FBS4* transcriptional levels in transgenic plants
The relative *FBS4* gene transcriptional levels in multiple transgenic lines were checked by RT-qPCR, comparing with the F-BOX STRESS-INDUCED 4 (FBS4) transcript in non-transformed Col plants. Data represents the mean ± *SD* ($n = 16$). No significant difference of *FBS4* expression is found between line #11, line #4, and line #5 after Student's *t*-test statistical analysis. RT-qPCR, reverse-transcription quantitative polymerase chain reaction.
Figure S16. Quantitative analysis of *FBS4* expression level and phenotype in *FBS4:gFBS4 flp-1* line #17 transgenic plants
(**A**) The *FBS4* transcriptional levels in *flp-1* and *FBS4:gFBS4 flp-1* transgenic line #17 were checked by RT-qPCR. (**B**) Quantitative analysis of the cluster size in *flp-1* and *FBS4:gFBS4 flp-1* line #17. Comparing with line #4 (see Figure 4G), the effect of *FBS4* expression on the formation of stomatal clusters in *flp-1* is limited in line #17. Data represents the mean ± *SD* ($n = 25$). RT-qPCR, reverse-transcription quantitative polymerase chain reaction.
Figure S17. Generation of *CYCA2;3*^{CRISPR} mutant
Diagram showing the target and mutated sites of *cyca2;3*^{CRISPR} by clustered regularly interspaced palindromic repeats (CRISPR)/CRISPR-associated protein 9 (Cas9) technology. The genomic RNA (gRNA) sequences within the second exon of *CYCA2;3* are indicated with underline. Protospacer adjacent motif sequences are labeled in green.
Figure S18. The proteasome inhibitor MG132 stabilizes CYCA2;3-GFP (green fluorescent protein) in root tips
(**A**) The GFP signals in 5 d after plating (DAP) root tip of *XVE:CYCA2;3-GFP* after induction. (**B**) Application of 26S Proteasome Inhibitor MG132 increases the GFP signals in a root tip of *XVE:CYCA2;3-GFP*. Green, GFP; purple, cell outlines are counterstained with propidium iodide. Scale bars, 50 μm.
Figure S19. Quantitative and statistical analysis of the fluorescent intensities of CYCA2;3-GFP (green fluorescent protein) that co-expressed with F-BOX STRESS-INDUCED 4 (FBS4)
Co-expression with *MYC-FBS4*, but not with mutated *MYC-FBS4*$^{\triangle F\text{-}box}$, dramatically reduced the fluorescence intensity of CYCA2;3-GFP, relative to the intensity level of CYCA2;3-GFP co-expressed with MYC. The experiment was repeated three times with similar results. Data are means ± *SD* ($n = 30$). Asterisks indicate the significant difference after Student's *t*-test, $^{**}P < 0.01$.
Figure S20. Quantitative analysis of CYCA2;3-GFP (green fluorescent protein) fluorescent intensity in roots
(**A**) Relative intensity of CYCA2;3-GFP signals in the epidermal cells of elongation zone in Col and *fbs4-1* roots. (**B**) Relative intensity of CYCA2;3-GFP signals in the root caps of Col and *fbs4-1*. The experiment was repeated three times with similar results. Data are means ± *SD* ($n = 46$). Asterisks indicate significant differences between Col and *fbs4-1* (Student's *t*-test, $^{**}P < 0.01$).
Figure S21. DNA ploidy distribution profiles in Col and *fbs4-1* cotyledons
(**A, B**) Flow cytometric analysis of 11 d after pollination (DAP) Col and *fbs4-1* cotyledons. (**C**) Quantitative analysis DNA ploidy levels.
Figure S22. F-BOX STRESS-INDUCED 4 (FBS4) is not involved in root length regulation
Length of 6-DAP root meristematic zone. Additional mutations of *fbs4-1* and *flp-1* had no effect on the root meristematic zone length in *uvi4*. Data are means ± *SD* ($n \geq 15$). Letters above the columns indicate the statistical analysis results after Duncan's multiple range test ($P < 0.05$).
Table S1. List of primers used in this study

Scan using WeChat with your smartphone to view JIPB online

Scan with iPhone or iPad to view JIPB online